

A theoretical analysis of filament length fluctuations in actin and other polymers

Jifeng Hu · Hans G. Othmer

Received: 23 August 2010 / Revised: 7 December 2010 / Published online: 14 January 2011
© Springer-Verlag 2011

Abstract Control of the structure and dynamics of the actin cytoskeleton is essential for cell motility and for maintaining the structural integrity of cells. Central to understanding the control of these features is an understanding of the dynamics of actin filaments, first as isolated filaments, then as integrated networks, and finally as networks containing higher-order structures such as bundles, stress fibers and actomyosin complexes. It is known experimentally that single filaments can exhibit large fluctuations, but a detailed understanding of the transient dynamics involved is still lacking. Here we first study stochastic models of a general system involving two-monomer types that can be analyzed completely, and then we report stochastic simulations on the complete actin model with three monomer types. We systematically examine the transient behavior of filament length dynamics so as to gain a better understanding of the time scales involved in reaching a steady state. We predict the lifetime of a cap of one monomer type and obtain the mean and variance of the survival time of a cap at the filament end, which together determine the filament length fluctuations.

Keywords Actin dynamics · Stochastic processes · Random walks on combs

Mathematics Subject Classification (2000) 92C45 · 60G07 · 82C41

J. Hu
School of Mathematics, University of Minnesota, Minneapolis, MN 55455, USA
e-mail: jfhu@math.umn.edu

H. G. Othmer (✉)
School of Mathematics, Digital Technology Center, University of Minnesota,
Minneapolis, MN 55455, USA
e-mail: othmer@math.umn.edu

1 Introduction

1.1 Background

Actin is the most abundant protein in many cell types, and the regulation of actin filament dynamics is essential for numerous cellular processes, including locomotion, cytokinesis and phagocytosis. Actin is involved in most aspects of cellular motility in eukaryotes, and actin polymerization is used by pathogens such as *Listeria monocytogenes* to propel themselves within and between host cells. In solution actin can self-assemble into filaments, bundles and higher-dimensional structures, but in vivo the type of structure formed is tightly controlled by intracellular regulatory molecules and extracellular mechanical and chemical signals. Depending on the context and the signal, a variety of structures can be formed, ranging from microspikes and filopodia, to larger pseudopodia and broad lamellipodia. These structures, which are distinguished by their topology, filament lengths and dynamics, not only provide the tracking and binding sites for many signaling and motor molecules, but also directly generate the active force required for many cellular activities (Pollard and Borisy 2003). In lamellipodia actin forms a network at the leading edge, the structure of which is determined by the growth of actin filaments at the leading edge and the depolymerization of actin from the meshwork in the interior of the cell. The protrusion speed or maximal protrusive force is a function of the filament length distribution and its elongation rate, and is limited by the availability of actin monomers, hydrolysis of actin-bound nucleotides and loading (Carlsson 2008). Within the broader distributed lamellipodium, actin filaments form a dense 3D dendritic structure with the growing ends abutting the membrane. In filopodia filaments are aligned in parallel and elongate at their barbed ends and disassemble at the pointed ends, thereby leading to protrusion of a filopodium. The half-life of actin filaments in the lamellipodium ranges from around 20 s to 2 min (Theriot and Mitchison 1991) and is correlated with cell speed: turnover is more rapid in rapidly-moving cells than in slower ones (McGrath et al. 2000). In any case, the turnover of filaments is more than two orders of magnitude faster than the turnover of pure actin filaments in solution (Zigmond 1993), and the in vivo system is far from thermodynamic equilibrium and under tight control.

The finely-tuned control of the structure of the cytoskeleton, which comprises the actin network, molecular motors, stress fibers and microtubules, ensures both the structural integrity of a cell, and the ability to rapidly change that structure. The properties of the cytoskeleton are determined in part by the local monomer concentration and in part by the dynamic control of monomer access to barbed-ends that stems from the presence or absence of various cofactors. Fluctuations in the local structure of the actin network are reflected in local fluctuations of the membrane, which facilitates searching for the direction in which to move or grow (Ponti et al. 2004; Bugyi and Carlier 2010). A filament that is growing against a load does so at a slower rate, and in the tethered filament-load models filaments that are not pushing the membrane exert passive drag forces via the stretching of the tether, thus opposing membrane protrusion. The effective force that a group of filaments can exert is a complex function of the filament polymerization rate as regulated by monomer availability, monomer nucleotide types

and filament-surface attachment (Mogilner and Oster 1996; Dickinson et al. 2004). Experiments show that the length fluctuations of growing filaments can lower the maximal force compared with that exerted by an ensemble of filament of equal lengths (Marcy et al. 2004; Footer et al. 2007; Schaus and Borisy 2008).

Filaments can also exhibit large length fluctuations in the absence of a load on the growing end, due to the stochastic exchange of monomers between the filament and the monomer pool, but controlled studies of these fluctuations are relatively recent. The theoretical single-monomer-type polymerization model proposed by Oosawa and Asakura (1975) predicted that at the steady ‘treadmilling’ state, the filament length distribution undergoes a diffusion process at the rate k^- , the off rate of monomer at filament ends. Later, Hu et al. (2007) studied the length distribution in solutions of filaments and showed that in a deterministic single-state model—where only one monomer type is present—the instantaneous diffusion rate constant is the mean of the polymerization and depolymerization rates. That analysis identified and characterized four distinct regimes of polymerizing filaments. As will be shown later, in these models both the elongation rate and diffusion constant are linear functions of monomer concentration over the entire concentration range. However, Carlier et al. showed earlier that the growth rate of filaments can be described to first order by two distinct linear functions applicable in different regimes of monomer concentration (Carlier et al. 1986). Filaments depolymerize below a critical concentration, whereas above it filaments grow at a constant rate and the slope of the elongation rate below the critical concentration is higher than that above it. At the critical concentration the growth rate vanishes, and filaments treadmill. In a seminal experiment, Fujiwara et al. observed that individual filaments show surprisingly large length fluctuations in the treadmilling phase (Fujiwara et al. 2002), and other experiments confirmed this high diffusion rate (Kuhn and Pollard 2005). A stochastic simulation of the length fluctuations of a single filament, using recent kinetic data for filament growth, is shown in Fig. 1.

One sees there that the pointed end shrinks continuously, with relatively small fluctuations in the mean position of the end. However, there are large fluctuations at the barbed (upper) end of the filament. One sees in (b) that when the filament has an ATP cap it grows, and that it decreases rapidly when the end monomer contains ADP (see inset to (b) at ~ 232 s). Furthermore, a significant number of ADP-Pi monomers, in which both ADP and phosphate are still bound to the protein, survive to the pointed end in this realization.

The diffusion coefficient for the length fluctuations of a single filament measured by Fujiwara et al. is 30–45 times as large as the prediction of previous models based on a single monomer type, and raises the question as to how it can be explained. A number of possible explanations have been suggested (Fujiwara et al. 2002; Kuhn and Pollard 2005; Fass et al. 2008): firstly, because the on- and off-rates of G-ADP and G-ATP are different, secondly, because the depolymerization of actin may occur via oligomers instead of single monomers, and finally because of the inability to experimentally definitively track filaments due to the spatial fluctuations in the solutions. As others have suggested and we show later, the first explanation suffices.

There are other biopolymers that exhibit very dynamic and rapidly-changing structures that can quickly adapt to local conditions within and outside the cell. Microtubules are bundles of polymer filaments called protofilaments that are built of α - and

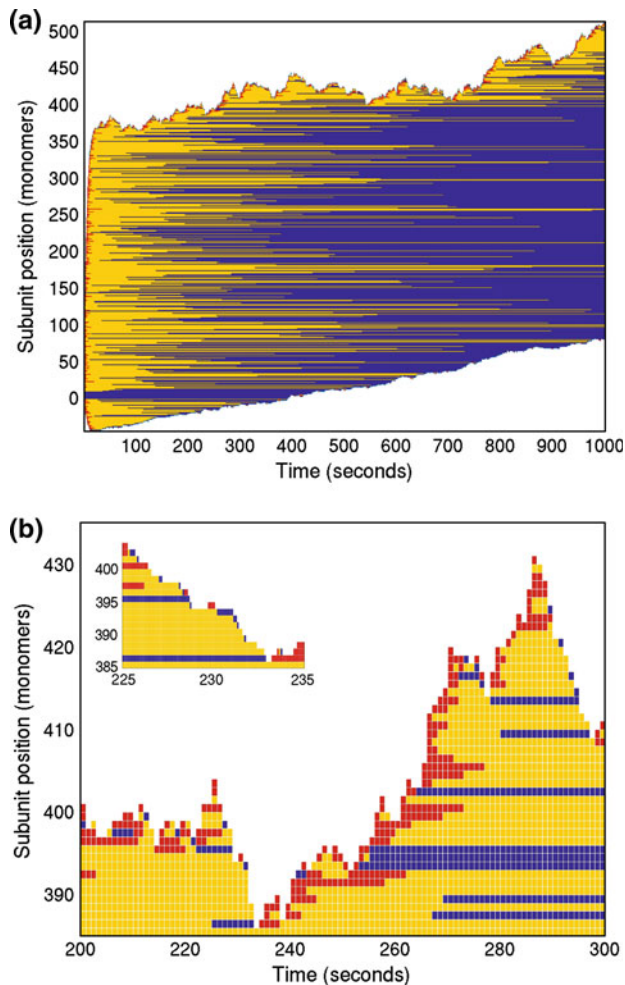


Fig. 1 **a** and **b** The length and nucleotide profile of a single filament during the polymerizing and treadmilling phase. Here the barbed end is at the *top* and the pointed end at the *bottom* — the former growing and the latter shrinking. *Black* represents an ADP-containing monomer, *gray* ADP-Pi, and *intermediate* ATP-containing monomers. These correspond to *blue*, *yellow* and *red* respectively in online version. Time in **(a)** and **(b)** is divided into 1-s steps, whereas in the inset to **(b)** it is divided into 0.1-s blocks. The simulation is based on the method described in [Matzavinos and Othmer \(2007\)](#) using the kinetic data in [Pollard \(2007\)](#) and shown in [Fig. 2](#). Initially 5,000 filaments consisting of 10 ADP-subunits polymerize in a 7.0 μM ATP actin monomer pool of 500 μm^3

β - tubulin dimers that polymerize into the protofilaments. In tubulin solutions microtubules exhibit what is called dynamic instability, in that they alternate rapidly between periods of growth and shrinking ([Mitchison and Kirschner 1984](#)). The ability to rapidly switch between growth and shrinking is thought to be essential for the random searching used to locate binding sites at the plasma membrane or on the nucleus, and in general is essential for the organization of the cell structure ([Tolic-Nørrelykke 2010](#)). The computational results given in [Fig. 1](#) for actin show large fluctuations at the

barbed end and suggest that it is the difference in the on- and off-rates of monomers with different associated nucleotides that may explain the dynamic switching between growth and shrinkage. In particular, the barbed-end dynamics reveal that elongation at that end requires an ATP-actin cap, but when the cap is lost the filament shrinks, more rapidly when the end monomer contains ADP. A similar explanation may apply to microtubules as well, since the switch-like behavior of microtubules depends on GTP hydrolysis. Most tubulin dimers in solution have GTP bound to their β -subunit, and the hydrolysis of this GTP to GDP is triggered by polymerization. While the on- and off-rates of the different monomers are not known, it is likely that the fluctuations have an explanation similar to that for actin filaments, even though there are 13 protofilaments in a microtubule and there may also be effects of mechanical stresses (VanBuren et al. 2005).

Other examples of biopolymer systems that show similar length fluctuations occur in bacterial plasmid segregation, where ParM forms bundles that have intrinsic dynamic instability (Popp et al. 2007), and in dendritic spines, where changes in their shape and size are correlated with the strength of excitatory synaptic connections and involve remodeling of the underlying actin cytoskeleton in a spine (Hotulainen and Hoogenraad 2010).

1.2 Previous models and analysis

Hill (1986) developed a deterministic model of cap formation, but only analyzed the steady state behavior and did not address the length fluctuations. Vavylonis et al. (2005) analyzed the growth of a single filament polymerizing in a constant monomer pool and showed that the diffusion constant first grows rapidly and then drops sharply as the critical monomer concentration is approached from below, as shown in Fig. 3. Using a two-state model, they predicted a sharp tooth-shaped diffusion coefficient versus concentration curve, which qualitatively matches with that with simulations using three monomer types. Later, Stukalin and Kolomeisky analyzed the long-time dynamics and predicted a large diffusion constant under the assumptions that hydrolysis in the filament is vectorial and that the ratio $q = k_{TC}/(w_T + r_h)$, which is a measure of the probability of having an actin cap, is less than one. Here c is the ATP-actin concentration, k_{TC} is the monomer on-rate, w_T is the off-rate, and r_h is the hydrolysis rate (Stukalin and Kolomeisky 2006). Recently, Ranjith et al. re-analyzed this model and identified a new dynamical phase of filament growth called the bounded growth phase, in addition to two previously-known unbounded growth phases (Ranjith et al. 2009). This analysis has been extended, again in the long-time regime, to incorporate dynamics at both ends of a filament and to compare the effect of vectorial versus random hydrolysis of ATP (Ranjith et al. 2010).

Our objective is to systematically examine the *transient* behavior of filament length dynamics so as to gain a better understanding of the time scales involved in reaching the asymptotic results obtained by others. First, we consider the filament dynamics in the single-state model. The filament elongation rate and diffusion constants are explicitly calculated when single or multiple filaments polymerize in a closed or open system. Then we present the two-state model, which is formally the same as in (Ranjith et al. 2009), but we obtain an analytical solution for a more general Markov jump process

in a two-dimensional state space, of which the actin model is a special case. The asymptotic behavior of the filament length fluctuation is related to the dynamics of the ATP cap at the filament end. We predict the lifetime of a cap and obtain the mean and variance of the survival time of a cap at the filament end, which together determine the filament length fluctuations. Our general 2D stochastic model can also be applied to the dynamics of other polymers such as microtubules, and to other Markov jump processes in 2D, including the diffusion of molecules in a comb-shaped environment or diffusing particles that become immobilized by binding to receptors or other binding sites. We indicate some of these extensions in the Sect. 6.

2 The single monomer type model

To prove the necessity of having multiple states or types for the monomers, we first analyze filament growth when the monomers are of a single type: first in a closed system for which the total number of actin monomers is conserved, and then in an open system in which the monomer concentration is fixed. Thus filaments are composed of single-state subunits, and elongate at a rate that is linearly dependent on the monomer concentration. The addition and disassociation rate of monomers are k^+ and k^- , respectively. (If one end is capped, k^+ and k^- refer to the rate constants at the free end; if both ends are free, they refer to the summed on- and off- rates for both ends.) For the single-state filament model, the critical concentration of monomers at which the net filament growth vanishes is thus $c_{crit} = k^-/k^+$. Some of the results in this section are well-known, but we give them for completeness and later comparison.

2.1 A closed system with a single filament

Suppose a single filament polymerizes in a solution of volume V_0 . The filament consists of l_0 subunits, and there are m_0 monomers in the solution. Let $q(n, t)$ denote the probability of monomer pool having n monomers at time t , $p(n, t)$ be the probability of the filament being of length n at time t , and let $N = l_0 + m_0$ be the total number of monomers. Under mass action kinetics the evolution equation for $q(n, t)$ is

$$\frac{dq(0, t)}{dt} = -\lambda q(0, t) + \mu q(1, t) \quad (1)$$

$$\begin{aligned} \frac{dq(n, t)}{dt} = & \lambda q(n-1, t) - (\lambda + n\mu) q(n, t) \\ & + (n+1)\mu q(n+1, t) \quad (1 \leq n \leq N-1) \end{aligned} \quad (2)$$

$$\frac{dq(N, t)}{dt} = \lambda q(N-1, t) - N\mu q(N, t) \quad (3)$$

where

$$\lambda = k^-, \quad \mu = k^+ / (\mathcal{N}_A \cdot V_0)$$

and \mathcal{N}_A is the Avogadro's number.

One finds that the steady-state monomer distribution is

$$q_\infty(n) = \lim_{t \rightarrow \infty} q(n, t) = \frac{1}{n!} \left(\frac{\lambda}{\mu}\right)^n / \left(\sum_{k=0}^N \frac{1}{k!} \left(\frac{\lambda}{\mu}\right)^k\right) \tag{4}$$

and $p_\infty(n) = q_\infty(N - n)$.¹ The mean and variance of the distribution are

$$M_\infty = \sum_{n=0}^N n q_\infty(n) = \frac{\lambda}{\mu} \left[1 - \frac{1}{N!} \left(\frac{\lambda}{\mu}\right)^N / \left(\sum_{k=0}^N \frac{1}{k!} \left(\frac{\lambda}{\mu}\right)^k\right) \right] \tag{5}$$

$$\begin{aligned} \sigma_\infty^2 &= \sum_{n=0}^N n^2 q_\infty(n) - \left(\sum_{n=0}^N n q_\infty(n)\right)^2 \\ &= \frac{\lambda}{\mu} - \left(\frac{\lambda}{\mu}\right)^2 \left(\frac{\frac{1}{N!} \left(\frac{\lambda}{\mu}\right)^N}{\sum_{k=0}^N \frac{1}{k!} \left(\frac{\lambda}{\mu}\right)^k} \right)^2 \\ &\quad + \frac{\frac{1}{N!} \left(\frac{\lambda}{\mu}\right)^N - \frac{1}{(N-1)!} \left(\frac{\lambda}{\mu}\right)^{N-1} - \frac{1}{N!} \left(\frac{\lambda}{\mu}\right)^{N-1}}{\sum_{k=0}^N \frac{1}{k!} \left(\frac{\lambda}{\mu}\right)^k} \left(\frac{\lambda}{\mu}\right)^2 \end{aligned} \tag{6}$$

Since

$$\sum_{k=0}^N \frac{1}{k!} \left(\frac{\lambda}{\mu}\right)^k \rightarrow e^{-\lambda/\mu}, \quad \text{as } N \rightarrow \infty$$

the steady-state monomer distribution tends to a Poisson distribution for large N with mean λ/μ , which is the monomer number at the critical concentration.

When N is sufficiently large, we can approximate the transient dynamics of the monomer pool as a random walk on the non-negative integers $\mathcal{Z}^+ = \{0, 1, 2, \dots\}$, and the evolution equations for $q(n, t)$ are now

$$\frac{dq(0, t)}{dt} = -\lambda q(0, t) + \mu q(1, t) \tag{7}$$

$$\frac{dq(n, t)}{dt} = \lambda q(n - 1, t) - (\lambda + n\mu) q(n, t) + (n + 1)\mu q(n + 1, t) \quad \text{for } n \geq 1 \tag{8}$$

¹ Note that this is not a simple binomial distribution, since the transition rates depend on the number of monomers.

If there are i_0 monomers initially

$$q(i_0, 0) = 1, \quad q(n, 0) = 0 \quad \text{for } n \neq i_0 \quad (9)$$

We obtain the solution by the method of generating functions and find that

$$q(n, t) = (\lambda/\mu)^n (1 - e^{-\mu t})^{n+i_0} e^{-(\lambda/\mu)(1-e^{-\mu t})} \\ \times \sum_{j=0}^{\min\{n, i_0\}} \frac{(\lambda/\mu)^{-j} e^{-j\mu t} (1 - e^{-\mu t})^{-2j}}{(n-j)!} \binom{i_0}{j} \quad (10)$$

The evolution of the mean and variance of $q(n, t)$ are

$$M(t) = (\lambda/\mu)(1 - e^{-\mu t}) + i_0 e^{-\mu t} \quad (11)$$

$$\sigma^2(t) = (\lambda/\mu + i_0 e^{-\mu t})(1 - e^{-\mu t}) \quad (12)$$

and the diffusion rate constant is

$$D(t) = \frac{1}{2} \frac{d\sigma^2(t)}{dt} = \lambda + 2i_0\mu e^{-2\mu t}$$

which coincides with the value predicted by [Oosawa and Asakura \(1975\)](#) in the limit $t \rightarrow \infty$.

For the special case of $i_0 = 0$, i.e., if we begin with a filament, the distribution is a Poisson distribution for all time

$$q(n, t) = \frac{1}{n!} \left(\frac{\lambda}{\mu} (1 - e^{-\mu t}) \right)^n e^{-\frac{\lambda}{\mu}(1-e^{-\mu t})}, \quad n \in \mathcal{N} \quad (13)$$

and in either case the asymptotic distribution as $t \rightarrow \infty$ is

$$q_\infty(n) = \frac{1}{n!} \left(\frac{\lambda}{\mu} \right)^n e^{-\lambda/\mu} \quad (14)$$

Therefore the steady-state distribution is always a Poisson distribution with mean λ/μ .

2.2 A closed system with multiple filaments

Next we begin with N_f filaments, all of length l_0 in subunits, immersed in a solution which contains no monomers. Let $q(m, t)$ be the probability of having m monomers at time t , and $p(n, t)$ the probability of a filament being of relative length n at time t . The relative length is defined as the length difference between the current filament length at time t versus the length at $t = 0$. We are interested in the filament length fluctuations on a time scale when no filaments disappear completely. As will be shown, when the total monomer concentration is above the critical value, the mean and variance of the monomer and filament length distributions stabilize before any filaments disappear.

Since it is supposed that the initial filament length is large enough, hereafter we approximate the dynamics of the system by assuming the relative length $n \in \mathcal{Z} = \{\dots, -1, 0, 1, \dots\}$. The evolution of the monomer distribution then satisfies the system

$$\frac{dq(0, t)}{dt} = -\lambda N_f q(0, t) + \mu N_f q(1, t) \quad (15)$$

$$\begin{aligned} \frac{dq(m, t)}{dt} &= \lambda N_f q(m-1, t) - (\lambda + m\mu) N_f q(m, t) \\ &\quad + (m+1)\mu N_f q(m+1, t), \quad m \geq 1 \end{aligned} \quad (16)$$

and the initial condition is

$$q(0, 0) = 1, \quad \text{and} \quad q(m, 0) = 0 \quad \text{for } m \geq 1 \quad (17)$$

One easily finds that the monomer distribution is as given in Eq. (13)

$$q(m, t) = \frac{1}{m!} \left[\frac{\lambda}{\mu} (1 - e^{-\mu N_f t}) \right]^m e^{-\lambda/\mu (1 - e^{-\mu N_f t})} \quad (18)$$

and as before

$$q_\infty(m) = \frac{1}{m!} \left(\frac{\lambda}{\mu} \right)^m e^{-\lambda/\mu} \quad (19)$$

Thus the monomer pool approaches the same distribution for multiple filaments as for the single filament, but at a rate that is N_f times as fast. The evolution of the filament length distribution, $p(n, t)$, is given by

$$\begin{aligned} \frac{dp(n, t)}{dt} &= \mu \left(\sum_{m=0}^{\infty} m q(m, t) \right) p(n-1, t) + \lambda p(n+1, t) \\ &\quad - \left[\mu \left(\sum_{m=0}^{\infty} m q(m, t) \right) + \lambda \right] p(n, t), \quad n \in \mathcal{Z} \end{aligned} \quad (20)$$

with the initial condition

$$p(0, 0) = 1, \quad \text{and} \quad p(n, 0) = 0 \quad \text{for } n \neq 0 \quad (21)$$

Equation (18) gives

$$\sum_{m=0}^{\infty} m q(m, t) = \lambda/\mu \cdot (1 - e^{-\mu N_f t}) \quad (22)$$

and one can then solve the system (20), (21) to obtain

$$p(n, t) = e^{-2\lambda t + \frac{\lambda}{\mu N_f}(1 - e^{-\mu N_f t})} \sum_{k=0}^{\infty} \frac{\left(-\frac{\lambda}{\mu N_f}(1 - e^{-\mu N_f t})\right)^k}{k!} I_{n-k}(2\lambda t) \quad (23)$$

where $I_n(z)$ is the modified Bessel function of the first kind. Using either this solution or the evolution equations directly, one can show that the first two moments of $p(n, t)$ are

$$\sum_{n=-\infty}^{\infty} n p(n, t) = -\frac{\lambda}{\mu N_f}(1 - e^{-\mu N_f t}) \quad (24)$$

$$\sum_{n=-\infty}^{\infty} n^2 p(n, t) = 2\lambda t + \left(\frac{\lambda}{\mu N_f}(1 - e^{-\mu N_f t})\right)^2 - \frac{\lambda}{\mu N_f}(1 - e^{-\mu N_f t}) \quad (25)$$

Therefore, the mean and variance of the filament lengths are

$$M(t) = -\frac{\lambda}{\mu N_f}(1 - e^{-\mu N_f t}) \quad (26)$$

$$\sigma^2(t) = 2\lambda t - \frac{\lambda}{\mu N_f}(1 - e^{-\mu N_f t}) \quad (27)$$

and thus the time-dependent diffusion rate constant is

$$D(t) = \frac{1}{2} \frac{d\sigma^2(t)}{dt} = \lambda \left(1 - \frac{1}{2} e^{-\mu N_f t}\right) \quad (28)$$

At large times the mean filament length approaches a constant, whereas the variance grows linearly with time. Both the mean length and the diffusion coefficient relax to their asymptotic value on a time scale of $T_1 = 1/(\mu N_f)$. A filament of length l_0 disappears on a time scale of $T_2 = l_0/k^-$. The necessary condition required for a stabilized filament length dynamics before filaments disappear is that $T_1 < T_2$, i.e. $l_0 N_f / (\mathcal{N}_A V_0) > k^- / k^+$, which means the total monomer concentration is above the critical value.

Thus with multiple filaments the monomer pool approaches a Poisson distribution as in the case of single filament system, but the filament length undergoes a diffusion process with the diffusion rate constant as k^- , which agrees with the diffusive phase of filament growth in a deterministic model studied in (Hu et al. 2007).

2.3 An open system with a fixed monomer bath

If instead of a fixed total monomer concentration let consider polymerization in a constant monomer bath of concentration c , then the dynamics of the probability of the

filament with relative length of n subunits at time t , $p(n, t)$, is

$$\frac{dp(n, t)}{dt} = k^+ c p(n-1, t) + k^- p(n+1, t) - (k^+ c + k^-) p(n, t) \quad (29)$$

Since the monomer constant the filaments do not interact with one another via the pool, and the evolution of the length distribution is a standard birth-death process with rates of $k^+ c$ and k^- , respectively. The mean and variance of the filament length distribution are

$$M(t) = (k^+ c - k^-) t \quad (30)$$

$$\sigma^2(t) = (k^+ c + k^-) t \quad (31)$$

and thus the diffusion rate constant is

$$D(c) = \frac{1}{2} \frac{d\sigma^2(t)}{dt} = \frac{k^+ c + k^-}{2} \quad (32)$$

Here both the mean and the variance increase linearly with time.

In summary, when multiple filaments polymerize in a closed system, the monomer pool approaches a Poisson distribution with parameter equal to the critical monomer number λ/μ for the given volume. The relaxation time τ for the monomer pool is linearly dependent on the filament numbers N_f and the solution volume V_0 as follows

$$\tau \sim \frac{\mathcal{N}_A V_0}{k^+ N_f}$$

The diffusion coefficient asymptotically approaches the monomer off-rate k^- . When a single filament polymerizes in a closed system, the monomer pool also approaches a Poisson distribution if N is large enough. If filaments are polymerizing in a constant monomer pool, the filament lengths undergo a convection-diffusion process with both mean and variance increasing linearly with time. In this case the diffusion coefficient is asymptotically proportional to a linear function of the fixed monomer concentration. Thus, whatever the configuration, the single-state filament model cannot reproduce the change in the growth rate and the non-monotonic behavior of the diffusion coefficient near the critical concentration that is observed experimentally.

3 The two-state filament model

3.1 The description of the side walk model

In the presence of sufficient ATP the displacement of ADP by ATP on actin monomers is rapid and nearly complete, and thus a solution of actin monomers comprises mainly G-ATP. In contrast, a sufficiently old filament is composed primarily of G-ADP (*cf.* Fig. 1). As shown in Fig. 2, the kinetic rates of G-ADP and G-ATP addition and release at filament ends are very different, and it has been proposed that the three distinct

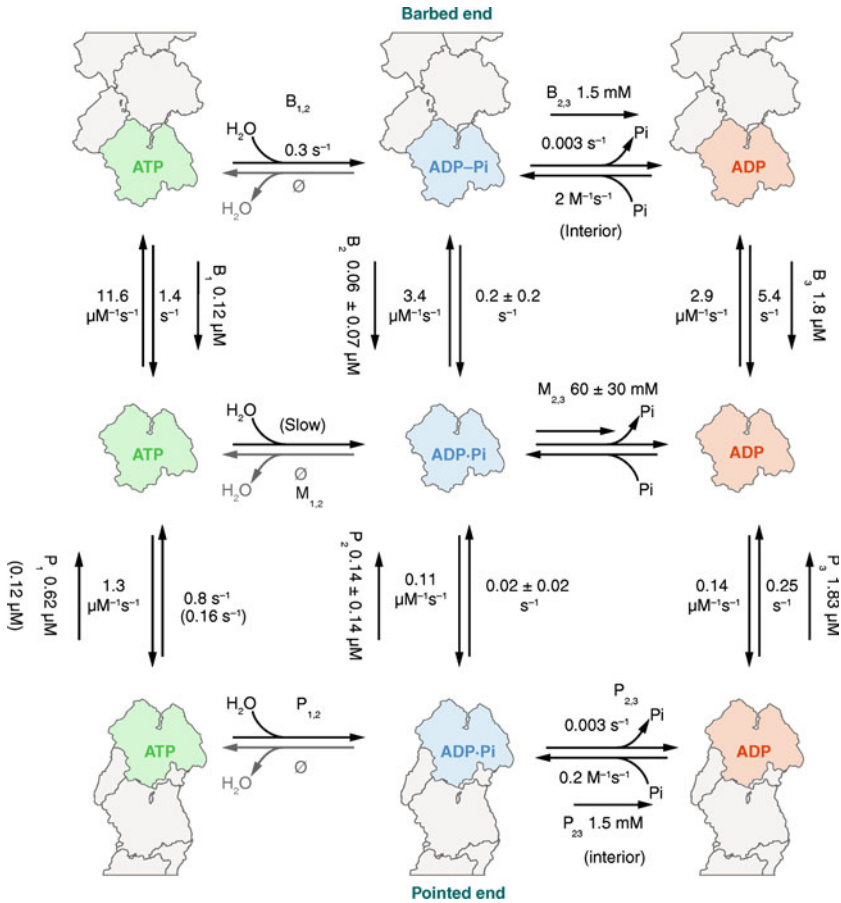


Fig. 2 The rates associated with addition and release of the three monomer types in actin polymerization. From Pollard (2007), with permission

capping states of the filament tip, as illustrated in Fig. 1, contribute to the non-monotonic behavior (Fujiwara et al. 2002; Kuhn and Pollard 2005). Here we investigate a two-state polymerization model wherein the nucleotide in either monomeric or filamentous actin is either ATP or ADP. Initially we do not include the transition of G-ATP to G-ADP relevant for actin, but later we take into account the possible influence of vectorial ATP hydrolysis by lumping the reactions from G-ATP to G-ADP into one first-order reaction, thereby neglecting the intermediate G-ADP-Pi state. It is reported that a G-ADP-Pi monomer at the filament tip releases its phosphate faster than when it is in the interior of a filament (Fujiwara et al. 2007), which suggests that most G-ADP-Pi monomers will become G-ADP monomers before they either disassociate from a filament end or are internalized via addition of another monomer. However, the realization of filament growth shown the inset of Fig. 1b shows that G-ADP-Pi can persist at the tip.

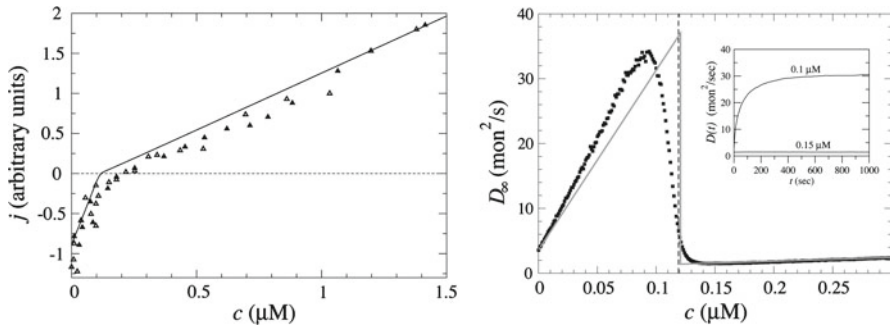


Fig. 3 The elongation rate and diffusion constant of filament lengths as functions of the monomer concentration (from Vavylonis et al. (2005) with permission)

In the following we consider a more general two-state polymer growth model, and for simplicity we consider the dynamics at one end. Suppose that a filament is immersed in a mixture of type B and type A monomers, both of which bind reversibly to the polymer. However, when a type A monomer is at the filament end no type B monomer can bind: thus A serves as a cap with respect to B (cf. Fig. 4a). As a result the polymer can have at most two non-overlapping regions: a type A portion and a type B portion, and the polymer length is the sum of the lengths of these portions. The polymer state is uniquely determined by (m, n) , where m and n are the lengths in monomers of the type A and B segments, respectively. Let $p(m, n, t)$ denote the probability of the polymer with configuration (m, n) at time t . The transition steps and rate between the various configurations are depicted in Fig. 4b. The on- and off-rates of type-A and type-B monomers are (α, β) and (r, s) , respectively. The length m of the type A segment is a non-negative integer, and increases or decreases by one following a horizontal step, during which n is unchanged. Vertical steps of one unit are allowed only when the polymer is free of any type A cap, i.e., when $m = 0$. As in Sect. 2.2, we assume that $n \in \mathcal{Z}$, since we deal with sufficiently long filaments, and are interested in the elongation and length fluctuation before the filament depolymerizes completely. To describe the reactions easily, we designate transitions along the vertical axis ($m = 0$) as the main walk, whereas the horizontal transitions comprise the side walk. If the side walk is limited to one step—i.e., $m = 0$ or 1, this model can be applied to model the translocation of a molecule diffusing and possibly drifting in a fluid environment and subject to receptor binding at the boundary. The specific experimental setting we address later is similar to that in Stukalin and Kolomeisky (2006), Ranjith et al. (2009)—a long ADP-filament polymerizing only at its barbed end in a constant G-ATP pool. However, we obtain both the transient and the asymptotic behavior of the filament lengths, and our primary concern there is the transient and asymptotic behavior of filament length fluctuations around the critical concentration of G-ATP.

We point out that this two-state polymer model is not applicable to actin filament polymerization in general, since the addition of actin monomers does not depend on the end state. However, the assumption that only a constant G-ATP is available in the monomer pool simplifies the filament growth, and reduces it to a special case of the two-state polymer model, where type A and B monomers are G-ATP and G-ADP,

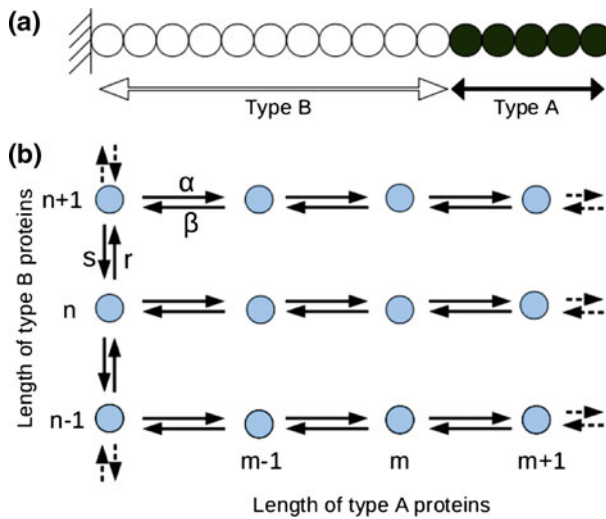


Fig. 4 **a** The schematic of a polymer with a core of type B monomers and a cap of type A monomers. **b** Each point of the grid (m, n) represents a polymer state, where m, n are the lengths of type A and B, respectively. (α, β, r, s) are kinetic rate constants for the reactions

respectively, and accordingly the parameters are

$$\alpha = k_T^+ c, \quad \beta = k_T^-, \quad s = k_D^-, \quad r = 0$$

where c is the G-ATP concentration, k_D^- the off-rate constant for G-ADP, and k_T^+, k_T^- are the on- and off-rate constants for G-ATP.

In view of the above description, the polymer configuration, $p(m, n, t)$, evolves according to

$$\begin{aligned} \frac{dp(0, n, t)}{dt} &= -\alpha p(0, n, t) + \beta p(1, n, t) - (r + s) p(0, n, t) \\ &\quad + r p(0, n - 1, t) + s p(0, n + 1, t) \end{aligned} \tag{33}$$

$$\begin{aligned} \frac{dp(m, n, t)}{dt} &= \alpha p(m - 1, n, t) + \beta p(m + 1, n, t) \\ &\quad - (\alpha + \beta) p(m, n, t) \quad (m \geq 1) \end{aligned} \tag{34}$$

As a first step toward deriving the dynamic behavior of the first and second moments of the polymer length distribution, we define the probability of the filament having an A-cap of length m and the mean length of the B segment for such a filament as

$$P_m(t) = \sum_{n=-\infty}^{\infty} p(m, n, t), \quad L_m(t) = \sum_{n=-\infty}^{\infty} n p(m, n, t) \tag{35}$$

where $m \in \mathbb{Z}^+$. According to Eqs. (33) and (34), they satisfy

$$\frac{dP_0(t)}{dt} = -\alpha P_0(t) + \beta P_1(t) \tag{36}$$

$$\frac{dP_m(t)}{dt} = \alpha P_{m-1}(t) + \beta P_{m+1}(t) - (\alpha + \beta) P_m(t) \quad (m \geq 1) \tag{37}$$

and

$$\frac{dL_0(t)}{dt} = -\alpha L_0(t) + \beta L_1(t) + (r - s) P_0(t) \tag{38}$$

$$\frac{dL_m(t)}{dt} = \alpha L_{m-1}(t) + \beta L_{m+1}(t) - (\alpha + \beta) L_m(t) \quad (m \geq 1) \tag{39}$$

The extra $P_0(t)$ term in the dynamics of $L_0(t)$ is due to loss of B monomer when an A-cap is removed from the polymer. Assuming that the polymer is initially composed of l_0 type B monomers alone, the initial condition becomes

$$P_0(0) = 1, \quad P_m(0) = 0 \quad (m \geq 1) \tag{40}$$

$$L_0(0) = l_0, \quad L_m(0) = 0 \quad (m \geq 1) \tag{41}$$

3.2 The solution for the P_m 's and L_m 's

As will be shown in the next section, the transient behavior of the mean and variance of the filament length depends on $P_0(t)$ and $L_0(t)$, so we must solve (36)–(41) first. P_m can be represented explicitly in terms of modified Bessel functions as follows (Goel and Richter-Dyn 1974):

$$P_m(t) = \rho^{m/2} e^{-(\alpha+\beta)t} \left(I_m(\omega t) + \rho^{-1/2} I_{m+1}(\omega t) + (1 - \rho) \sum_{k=2}^{\infty} \rho^{-k/2} I_{m+k}(\omega t) \right) \tag{42}$$

where $\rho = \alpha/\beta$, $\omega = 2\sqrt{\alpha\beta}$, and $I_m(z)$ is a modified Bessel function of the first kind. In particular, we have

$$P_0(t) = e^{-(\alpha+\beta)t} \left(I_0 + \rho^{-1/2} I_1 + (1 - \rho) \sum_{k=2}^{\infty} \rho^{-k/2} I_k \right) \tag{43}$$

where for simplification the variable ωt of I_n is suppressed hereafter unless otherwise specified.

To solve for the L_m 's, we first nondimensionalize the L_m 's by the change of variables

$$K_m(t) = L_m(t)/l_0 \tag{44}$$

and then the K_m 's solve

$$\frac{dK_m(t)}{dt} = \alpha K_{m-1}(t) + \beta K_{m+1}(t) - (\alpha + \beta) K_m(t) \quad (m \geq 1) \quad (45)$$

$$\frac{dK_0(t)}{dt} = -\alpha K_0(t) + \beta K_1(t) + (r - s) P_0(t)/l_0 \quad (46)$$

with the initial condition

$$K_0(0) = 1, \quad K_m(0) = 0 \quad (m \geq 1)$$

The term involving P_0 enters as a nonhomogeneous term in (46), which complicates the solution of the system and precludes use of a generating function. To circumvent this, we extend the process symmetrically to \mathcal{Z} , using (45), and later impose conditions that guarantee that (46) is satisfied. As a first step we introduce as yet undetermined initial conditions for the extended process as

$$K_{-m}(0) = d_m \quad (m \geq 1). \quad (47)$$

The generating function for the extended process is

$$G(z, t) = \sum_{m=-\infty}^{\infty} K_m(t) z^m \quad (48)$$

and this satisfies

$$\frac{\partial G(z, t)}{\partial t} = (z - 1)(\alpha - \beta/z) G(z, t) \quad (49)$$

$$G(z, 0) = 1 + \sum_{m=1}^{\infty} d_m z^{-m} \quad (50)$$

The general solution to (49) is

$$G(z, t) = \phi(z) e^{-(\alpha+\beta)t} \sum_{m=-\infty}^{\infty} \rho^{m/2} I_m z^m \quad (51)$$

and, using the fact that $I_0(0) = 1$ and $I_k(0) = 0$ for $k \neq 1$, the initial condition implies that

$$\phi(z) = 1 + \sum_{m=1}^{\infty} d_m z^{-m} \quad (52)$$

To solve for the K_m 's, which are the coefficients of the powers of z in (48), we have to find the d_m 's. To ensure that the evolution equation for K_0 is the same in the original

and extended system we must impose the condition

$$\alpha K_{-1}(t) - \beta K_0(t) = (r - s)P_0(t)/l_0 \tag{53}$$

Since $K_{-1}(t)$ and $K_0(t)$ are the coefficients of the terms containing z^{-1} and z^0 in (51), we have

$$K_0(t) = \left(I_0 + \sum_{k=1}^{\infty} d_k I_k \rho^{\frac{k}{2}} \right) e^{-(\alpha+\beta)t} \tag{54}$$

$$K_{-1}(t) = \left(\rho^{-\frac{1}{2}} I_1 + \sum_{k=1}^{\infty} d_k I_{k-1} \rho^{\frac{k-1}{2}} \right) e^{-(\alpha+\beta)t} \tag{55}$$

Using these and P_0 in (53), one obtains

$$\begin{aligned} & \beta \left((\rho d_1 - 1) I_0 + \rho^{\frac{1}{2}} (\rho d_2 + 1 - d_1) I_1 + \sum_{k=2}^{\infty} \rho^{\frac{k}{2}} (\rho d_{k+1} - d_k) I_k \right) \\ &= \frac{r-s}{l_0} \left(I_0 + \rho^{-\frac{1}{2}} I_1 + (1-\rho) \sum_{k=2}^{\infty} \rho^{-\frac{k}{2}} I_k \right) \end{aligned} \tag{56}$$

Since the equality holds for all t one can show, by successively differentiating the series, setting $t = 0$, and using properties of the Bessel functions, that the coefficients of the I_k 's must be identical on both sides of the equality for each k . As a result, one finds that

$$d_1 = \rho^{-1} \left(1 + \frac{1}{\beta} \frac{r-s}{l_0} \right) \tag{57}$$

$$d_k = \rho^{-k} \left(1 - \rho + \frac{2}{\beta} \frac{r-s}{l_0} + (k-2) \frac{1-\rho}{\beta} \frac{r-s}{l_0} \right) \quad (k \geq 2) \tag{58}$$

It follows from (51) and (52) that

$$K_m(t) = e^{-(\alpha+\beta)t} \left(\rho^{m/2} I_m + \sum_{k=1}^{\infty} d_k \rho^{(m+k)/2} I_{m+k} \right) \tag{59}$$

for $m \geq 0$, and therefore, using (57)–(58), one obtains the L_m 's as

$$\begin{aligned} L_m(t) = l_0 P_m(t) + \frac{r-s}{\beta} e^{-(\alpha+\beta)t} & \left(\rho^{(m-1)/2} I_{m+1} \right. \\ & \left. + 2\rho \sum_{k=2}^{\infty} \rho^{(m+k)/2} I_{m+k} + (1-\rho) \sum_{k=2}^{\infty} k \rho^{(m-k)/2} I_{m+k} \right) \end{aligned} \tag{60}$$

Together (42) and (60) give the complete evolution of the probability of an A-cap of length m and the mean length of the B-segment.

In particular, the mean length of filaments without an A-cap is

$$L_0(t) = l_0 P_0 + \frac{r-s}{\beta} e^{-(\alpha+\beta)t} \left(\rho^{-\frac{1}{2}} I_1 + 2\rho \sum_{k=2}^{\infty} \rho^{-\frac{k}{2}} I_k + (1-\rho) \sum_{k=2}^{\infty} \rho^{-\frac{k}{2}} k I_k \right) \tag{61}$$

Depending on the relative size of the on- and off-rate of A monomers, the dynamics of the P_m 's and the L_m 's have different qualitative and asymptotic behavior.

Case I: $\alpha \neq \beta$ When $\alpha < \beta$, i.e. the off-rate of A monomer is larger than the on-rate,

$$\lim_{t \rightarrow \infty} P_m(m, t) = P_m^\infty = \rho^m (1 - \rho) \tag{62}$$

while for $\alpha > \beta$,

$$\lim_{t \rightarrow \infty} P_m(m, t) = P_m^\infty = 0 \tag{63}$$

This corresponds to the case in which both the mean and variance grows linearly for the single-monomer model analyzed in the previous section. In addition, when $\alpha \neq \beta$, it can be shown (Doorn 2001) that $P_m(t)$ converges to its equilibrium exponentially at the rate

$$|P_m(t) - P_m^\infty| \leq C e^{-t(\alpha+\beta-2\sqrt{\alpha\beta})} \tag{64}$$

which shows that the relaxation time of $P_m(t)$ is of the order of

$$T_{1/2} = \left(\sqrt{\alpha} - \sqrt{\beta} \right)^{-2} \tag{65}$$

Thus the relaxation time is related to the difference between square roots of the on- and off-rate, which stems from the boundary effect in the system. When the on-rate approaches the off-rate linearly, i.e. $(\alpha - \beta)/\beta = \epsilon \rightarrow 0$, the relaxation time is

$$T_{1/2} \sim \frac{4}{\beta} \frac{1}{\epsilon^2}$$

For this special case where $\alpha \neq \beta$, $L_0(t)$ can be rewritten as

$$L_0(t) = l_0 P_0 + \frac{r-s}{\beta} \frac{2\rho}{1-\rho} P_0 + (r-s)(1-\rho) P_0 t - \frac{r-s}{\beta} e^{-(\alpha+\beta)t} \left(\frac{2\rho}{1-\rho} I_0 + \rho^{\frac{1}{2}} \frac{1+\rho}{1-\rho} I_1 \right) \tag{66}$$

Case II: $\alpha = \beta$ From Eq. (43), we have

$$P_0(t) = e^{-2\beta t} (I_0 + I_1) \tag{67}$$

and

$$P_0(t) \sim \frac{1}{\sqrt{\pi\beta t}} \rightarrow 0, \text{ as } t \rightarrow \infty \tag{68}$$

We also find that

$$P_m = e^{-2\beta t} (I_m + I_{m+1}) \tag{69}$$

$$L_m = I_0 P_m + \frac{r-s}{\beta} e^{-2\beta t} \left(I_{m+1} + 2 \sum_{k=2}^{\infty} I_{m+k} \right) \tag{70}$$

A comparison of the two cases shows that when $\alpha < \beta$ there is a finite probability of a cap of any length, whereas when $\alpha \geq \beta$ the probability of any finite cap length decays to zero. In the former case the cap size at long times is exponentially distributed.

3.3 The statistics of filament length elongation and diffusion

In order to quantify the statistics of the different segments of a filament or polymer, we define the following variables and analyze their transient evolution.

$$\begin{aligned} M_x(t) &= \sum_{m=0}^{\infty} \sum_{n=0}^{\infty} m p(m, n, t), & V_x(t) &= \sum_{m=0}^{\infty} \sum_{n=0}^{\infty} m^2 p(m, n, t) \\ M_y(t) &= \sum_{m=0}^{\infty} \sum_{n=0}^{\infty} n p(m, n, t), & V_y(t) &= \sum_{m=0}^{\infty} \sum_{n=0}^{\infty} n^2 p(m, n, t) \\ M_{x+y}(t) &= \sum_{m=0}^{\infty} \sum_{n=0}^{\infty} (m+n) p(m, n, t), & V_{x+y}(t) &= \sum_{m=0}^{\infty} \sum_{n=0}^{\infty} (m+n)^2 p(m, n, t) \end{aligned}$$

Some of these can be re-written in terms of known quantities as follows:

$$M_x(t) = \sum_{m=0}^{\infty} m P_m(t), \quad V_x(t) = \sum_{m=0}^{\infty} m^2 P_m(t), \quad M_y(t) = \sum_{m=0}^{\infty} L_m(t) \tag{71}$$

In view of (33)–(41), the time evolution of the above quantities are

$$\frac{dM_x(t)}{dt} = \alpha - \beta + \beta P_0(t) \tag{72}$$

$$\frac{dV_x(t)}{dt} = 2(\alpha - \beta)M_x(t) + \alpha + \beta - \beta P_0(t) \tag{73}$$

$$\frac{dM_y(t)}{dt} = (r - s) P_0(t) \quad (74)$$

$$\frac{dV_y(t)}{dt} = 2(r - s) L_0(t) + (r + s) P_0(t) \quad (75)$$

$$\frac{dM_{x+y}(t)}{dt} = (\alpha - \beta) + (\beta + r - s) P_0(t) \quad (76)$$

$$\begin{aligned} \frac{dV_{x+y}(t)}{dt} &= (\alpha + \beta) + 2r P_0(t) + 2(\alpha - \beta) M_{x+y}(t) \\ &\quad + (\beta + r - s) (2L_0(t) - P_0(t)) \end{aligned} \quad (77)$$

From these one obtains the evolution equations for the variances of these lengths as

$$\frac{d\sigma_x^2(t)}{dt} = \alpha + \beta - \beta P_0(t) (1 + 2M_x(t)) \quad (78)$$

$$\frac{d\sigma_y^2(t)}{dt} = (r + s) P_0(t) - 2(r - s) (M_y(t) P_0(t) - L_0(t)) \quad (79)$$

$$\frac{d\sigma_{x+y}^2(t)}{dt} = (\alpha + \beta) + (r + s - \beta) P_0 - 2(\beta + r - s) (M_{x+y} P_0 - L_0) \quad (80)$$

According to Eqs. (72), (74) and (76), we have

$$M_{x+y} = -\frac{\beta}{r-s} l_0 + (\alpha - \beta)t + \frac{\beta + r - s}{r-s} M_y \quad (81)$$

$$M_x = M_{x+y} - M_y \quad (82)$$

where M_y is given in (71).

When $\rho \neq 1$, i.e. $\alpha \neq \beta$, it follows from (60) and (71) that

$$\begin{aligned} M_y(t) &= l_0 - \frac{r-s}{\beta} \frac{1}{1-\rho} + \frac{r-s}{\beta} \frac{1+\rho}{1-\rho} \frac{P_0}{1-\rho} + (r-s) P_0 t \\ &\quad - \frac{r-s}{\beta} e^{-(\alpha+\beta)t} \left(\frac{2\rho}{(1-\rho)^2} I_0 + \rho^{\frac{1}{2}} \frac{1+\rho}{(1-\rho)^2} I_1 \right) \end{aligned} \quad (83)$$

and from Eq. (82)

$$\begin{aligned} M_x(t) &= \frac{1}{1-\rho} \left(\frac{1+\rho}{1-\rho} P_0 - 1 \right) + (\alpha - \beta + \beta P_0) t \\ &\quad - e^{-(\alpha+\beta)t} \left(\frac{2\rho}{(1-\rho)^2} I_0 + \rho^{\frac{1}{2}} \frac{1+\rho}{(1-\rho)^2} I_1 \right) \end{aligned} \quad (84)$$

Therefore,

$$\begin{aligned}
 M_y P_0 - L_0 = & -\frac{r-s}{\beta} \frac{\rho}{1-\rho} P_0 + \frac{r-s}{\beta} \frac{1+\rho}{1-\rho} \frac{P_0}{1-\rho} (P_0 - (1-\rho)) \\
 & + (r-s) (P_0 - (1-\rho)) P_0 t \\
 & - \frac{r-s}{\beta} e^{-(\alpha+\beta)t} (P_0 - (1-\rho)) \\
 & \times \left(\frac{2\rho}{(1-\rho)^2} I_0 + \rho^{\frac{1}{2}} \frac{1+\rho}{(1-\rho)^2} I_1 \right)
 \end{aligned} \tag{85}$$

and in addition

$$\begin{aligned}
 M_{x+y} P_0 - L_0 = & \frac{\beta-r+s}{\beta} \frac{\rho P_0}{1-\rho} + \frac{\beta+r-s}{\beta} \frac{1+\rho}{1-\rho} \frac{P_0}{1-\rho} (P_0 - (1-\rho)) \\
 & + (\alpha - \beta + \beta P_0) P_0 t + (r-s) (P_0 - (1-\rho)) P_0 t \\
 & - c_0 I_0 e^{-(\alpha+\beta)t} - c_1 I_1 e^{-(\alpha+\beta)t}
 \end{aligned} \tag{86}$$

where

$$c_0 = \frac{2\rho}{(1-\rho)^2} \left[P_0 + \frac{r-s}{\beta} (P_0 - (1-\rho)) \right] \tag{87}$$

$$c_1 = \frac{(1+\rho)\rho^{\frac{1}{2}}}{(1-\rho)^2} \left[P_0 + \frac{r-s}{\beta} (P_0 - (1-\rho)) \right] \tag{88}$$

As a result, we obtain the following for the transient elongation rate and the diffusion coefficient of various filament segments. The net fluxes are given by

$$j_x(t) \equiv \frac{dM_x(t)}{dt} = \alpha - \beta + \beta P_0(t) \tag{89}$$

$$j_y(t) \equiv \frac{dM_y(t)}{dt} = (r-s) P_0(t) \tag{90}$$

$$j_{x+y}(t) \equiv \frac{dM_{x+y}(t)}{dt} = \alpha - \beta + (\beta + r-s) P_0(t) \tag{91}$$

and the diffusion coefficients are given by

$$\begin{aligned}
 D_x(t) = & \frac{1}{2} \frac{d\sigma_x^2(t)}{dt} \\
 = & \frac{\alpha + \beta}{2} - \beta P_0 \left[\frac{1}{2} + \frac{1}{1-\rho} \left(\frac{1+\rho}{1-\rho} P_0 - 1 \right) + (\alpha - \beta + \beta P_0) t \right. \\
 & \left. - e^{-(\alpha+\beta)t} \left(\frac{2\rho}{(1-\rho)^2} I_0 + \rho^{\frac{1}{2}} \frac{1+\rho}{(1-\rho)^2} I_1 \right) \right]
 \end{aligned} \tag{92}$$

$$\begin{aligned}
 D_y(t) &= \frac{1}{2} \frac{d\sigma_y^2(t)}{dt} = \frac{(r+s)}{2} P_0 + (r-s)^2 \\
 &\times \left[\frac{\rho}{\beta(1-\rho)} P_0 - \frac{1+\rho}{\beta(1-\rho)} \frac{P_0}{1-\rho} (P_0 - (1-\rho)) \right. \\
 &\quad \left. - (P_0 - (1-\rho)) P_0 t + \frac{1}{\beta} e^{-(\alpha+\beta)t} (P_0 - (1-\rho)) \right. \\
 &\quad \left. \times \left(\frac{2\rho}{(1-\rho)^2} I_0 + \rho \frac{1}{2} \frac{1+\rho}{(1-\rho)^2} I_1 \right) \right] \tag{93}
 \end{aligned}$$

$$\begin{aligned}
 D_{x+y}(t) &= \frac{1}{2} \frac{d\sigma_{x+y}^2(t)}{dt} = \frac{\alpha+\beta}{2} + \frac{r+s-\beta}{2} P_0 - (\beta+r-s) \\
 &\times \left[\frac{\beta-r+s}{\beta} \frac{\rho P_0}{1-\rho} + \frac{\beta+r-s}{\beta} \frac{1+\rho}{1-\rho} \frac{P_0}{1-\rho} (P_0 - (1-\rho)) \right. \\
 &\quad \left. + (\alpha-\beta+\beta P_0) P_0 t + (r-s) (P_0 - (1-\rho)) P_0 t \right. \\
 &\quad \left. - c_0 I_0 e^{-(\alpha+\beta)t} - c_1 I_1 e^{-(\alpha+\beta)t} \right] \tag{94}
 \end{aligned}$$

Case I: $\alpha < \beta$ In this case the probabilities P_m of the cap sizes asymptotically approach their steady state value $\rho^m(1-\rho)$ given in (62). Therefore, the mean cap size relaxes to

$$\lim_{t \rightarrow \infty} M_x(t) = \sum_{m=0}^{\infty} m P_m^\infty = \frac{\alpha/\beta}{1-\alpha/\beta}$$

at large times. If $\alpha \neq \beta$, the modified Bessel functions have the asymptotic properties

$$t^m I_n(2\sqrt{\alpha\beta} t) e^{-(\alpha+\beta)t} \rightarrow 0, \text{ as } t \rightarrow \infty \tag{95}$$

for any fixed $m, n \in \mathbb{Z}^+$ (Abramowitz and Stegun 1965). Thus the transient elongation rate and the diffusion coefficient for the B-segment have the following asymptotic behavior

$$\lim_{t \rightarrow \infty} j_y(t) = (r-s)(1-\alpha/\beta) \tag{96}$$

$$\lim_{t \rightarrow \infty} D_y(t) = \frac{r+s}{2} \left(1 - \frac{\alpha}{\beta} \right) + \frac{(r-s)^2}{\beta} \frac{\alpha}{\beta} \tag{97}$$

and those for the complete filament are

$$\lim_{t \rightarrow \infty} j_{x+y}(t) = (r-s)(1-\alpha/\beta) \tag{98}$$

$$\lim_{t \rightarrow \infty} D_{x+y}(t) = \frac{r+s}{2} \left(1 - \frac{\alpha}{\beta} \right) + \frac{(r-s)^2}{\beta} \frac{\alpha}{\beta} \tag{99}$$

Thus

$$\lim_{t \rightarrow \infty} (M_{x+y}(t) - M_y(t)) = \lim_{t \rightarrow \infty} M_x(t) = \frac{\alpha/\beta}{1 - \alpha/\beta} \quad (100)$$

and

$$\lim_{t \rightarrow \infty} \left(\frac{d\sigma_{x+y}^2}{dt} - \frac{d\sigma_y^2}{dt} \right) = 0 \quad (101)$$

which implies that when the on-rate of A-monomer is less than its off-rate, the average cap size is finite at large times, and the diffusion of the total filament length results primarily from that of the B-segment.

Case II: $\alpha > \beta$ Since $\lim_{t \rightarrow \infty} P_0(t) = 0$ at an exponential rate as in (64) for $\alpha > \beta$, Eq. (72) gives the average cap growth rate

$$\lim_{t \rightarrow \infty} j_x(t) = \alpha - \beta \quad (102)$$

and Eq. (78) leads to

$$\lim_{t \rightarrow \infty} D_x(t) = \frac{\alpha + \beta}{2} \quad (103)$$

Using similar arguments as for the case of $\alpha < \beta$, we find that

$$\lim_{t \rightarrow \infty} j_{x+y}(t) = \alpha - \beta \quad (104)$$

$$\lim_{t \rightarrow \infty} D_{x+y}(t) = \frac{\alpha + \beta}{2} \quad (105)$$

Thus this is a degenerate case of the two-state polymer model, since at large times the B-core is never exposed, and the filament length fluctuation is due only to the A-cap. This result agrees with that from the single-state filament model.

Case III: $\alpha = \beta$ In the intermediate case of $\alpha = \beta$, the mean length of the A- and B-segments and the total filament length can be obtained from (69) and (70):

$$M_x(t) = -\frac{1}{2} + \frac{1}{2}e^{-2\beta t} I_0 + 2\beta t e^{-2\beta t} (I_0(2\beta t) + I_1(2\beta t)) \quad (106)$$

$$M_y(t) = l_0 - \frac{r-s}{2\beta} + \frac{r-s}{\beta} e^{-2\beta t} \left[\frac{1}{2} I_0 + 2\beta t (I_0 + I_1) \right] \quad (107)$$

$$\begin{aligned} M_{x+y}(t) &= l_0 - \frac{\beta + r - s}{2\beta} + \frac{\beta + r - s}{\beta} e^{-2\beta t} \\ &\quad \times \left[\frac{1}{2} I_0 + 2\beta t (I_0 + I_1) \right] \end{aligned} \quad (108)$$

From (68), we have the leading term of the large time approximation as

$$M_x(t) \sim \beta \sqrt{\frac{4}{\pi\beta}} t^{1/2}, \quad M_y(t) \sim (r-s) \sqrt{\frac{4}{\pi\beta}} t^{1/2} \quad (109)$$

$$M_{x+y}(t) \sim (\beta+r-s) \sqrt{\frac{4}{\pi\beta}} t^{1/2} \quad (110)$$

In addition,

$$\begin{aligned} M_y P_0 - L_0 &= -\frac{r-s}{\beta} (1 - P_0/2) \\ &\quad + \frac{r-s}{2\beta} e^{-2\beta t} I_0 + 2t(r-s) P_0^2 \end{aligned} \quad (111)$$

$$\begin{aligned} M_{x+y} P_0 - L_0 &= -\left(\frac{\beta-r+s}{2\beta} P_0 + \frac{r-s}{\beta} \right) + \frac{\beta+r-s}{\beta} P_0 \\ &\quad \times \left[e^{-2\beta t} I_0/2 + 2\beta t P_0 \right] \end{aligned} \quad (112)$$

where $P_0(t) = e^{-2\beta t} (I_0(2\beta t) + I_1(2\beta t))$. Accordingly, the transient elongation rate and diffusion coefficients are

$$j_x(t) = \beta e^{-2\beta t} (I_0(2\beta t) + I_1(2\beta t)) \quad (113)$$

$$j_y(t) = (r-s) e^{-2\beta t} (I_0(2\beta t) + I_1(2\beta t)) \quad (114)$$

$$j_{x+y}(t) = (\beta+r-s) e^{-2\beta t} (I_0(2\beta t) + I_1(2\beta t)) \quad (115)$$

$$\begin{aligned} D_x(t) &= \beta - \frac{\beta}{2} e^{-4\beta t} (I_0(2\beta t) + I_1(2\beta t)) \\ &\quad \times [I_0(2\beta t) + 4\beta t (I_0(2\beta t) + I_1(2\beta t))] \end{aligned} \quad (116)$$

$$\begin{aligned} D_y(t) &= \frac{(r+s)}{2} e^{-2\beta t} (I_0(2\beta t) + I_1(2\beta t)) \\ &\quad + \frac{(r-s)^2}{\beta} \left[1 - e^{-2\beta t} (I_0(2\beta t) + I_1(2\beta t)/2) \right. \\ &\quad \left. + 2\beta t e^{-4\beta t} (I_0(2\beta t) + I_1(2\beta t))^2 \right] \end{aligned} \quad (117)$$

$$\begin{aligned} D_{x+y}(t) &= -(r-s) + \left(\frac{r+s}{2} - \frac{(r-s)^2}{2\beta} \right) e^{-2\beta t} (I_0(2\beta t) + I_1(2\beta t)) \\ &\quad + \frac{(\beta+r-s)^2}{\beta} \left[1 - e^{-4\beta t} (I_0(2\beta t) + I_1(2\beta t)) \right. \\ &\quad \left. \times (I_0(2\beta t)/2 + 2\beta t (I_0(2\beta t) + I_1(2\beta t))) \right]. \end{aligned} \quad (118)$$

Therefore, at large times

$$\lim_{t \rightarrow \infty} j_x(t) = 0, \quad \lim_{t \rightarrow \infty} D_x(t) = \beta - (\beta + r - s) \left(\frac{2}{\pi} - \frac{r - s}{\beta} \right) \quad (119)$$

$$\lim_{t \rightarrow \infty} j_y(t) = 0, \quad \lim_{t \rightarrow \infty} D_y(t) = \left(1 - \frac{2}{\pi} \right) \frac{(r - s)^2}{\beta} \quad (120)$$

$$\begin{aligned} \lim_{t \rightarrow \infty} j_{x+y}(t) = 0, \quad \lim_{t \rightarrow \infty} D_{x+y}(t) = & -(r - s) \\ & + \frac{(\beta + r - s)^2}{\beta} \left(1 - \frac{2}{\pi} \right) \end{aligned} \quad (121)$$

Note that

$$\lim_{t \rightarrow \infty} D_x(t) \geq \left(2\sqrt{1 - 2/\pi} - (1 - 2/\pi) \right) |r - s| \geq 0 \quad (122)$$

$$\lim_{t \rightarrow \infty} D_{x+y}(t) \geq \left(3 - \frac{8}{\pi} \right) |r - s| \geq 0 \quad (123)$$

Therefore, when the on- and off-rates of A are equal, the mean length of the A-, B-segments and the total filament length increases as $t^{1/2}$ at large times as in (109), (110), so the time rate of change of mean filament length approaches zero as $t \rightarrow \infty$. Furthermore, the diffusion coefficients of all three lengths are constant at large times, as indicated by (119)–(121). As later simulation results show, the diffusion coefficient is generally discontinuous at $\alpha = \beta$, which can be seen from their limits when α approaches β from below and above:

$$D_- = \lim_{\alpha \rightarrow \beta^-} \lim_{t \rightarrow \infty} D_{x+y}(t) = \frac{(r - s)^2}{\beta} \quad (124)$$

$$D_+ = \lim_{\alpha \rightarrow \beta^+} \lim_{t \rightarrow \infty} D_{x+y}(t) = \beta. \quad (125)$$

In particular

$$\frac{D_-}{D_+} = \left(\frac{r - s}{\beta} \right)^2 \quad (126)$$

Therefore, when $|r - s| \geq \beta$, $D_- \geq D_+$; otherwise, $D_- < D_+$.

3.4 The lifetime of a cap

The foregoing results show how the presence of a cap influences the filament length fluctuations, and in this section we investigate how the lifetime of the cap is related to these fluctuations. In particular, we determine the distribution of the lifetime of a cap initially of length m_0 , and compute the first two moments of this distribution.

The cap size changes can be modeled as a biased random walk in \mathcal{Z}^+ , and because the lifetime of a cap is the time at which the walk hits $m = 0$, the length of the B-core

is irrelevant. Let $p(m, t)$ be the probability of a cap of initial length m_0 being of length m at time t . These evolve according to

$$\frac{dp(m, t)}{dt} = \alpha p(m-1, t) - (\alpha + \beta) p(m, t) + \beta p(m+1, t) \quad (127)$$

$$\frac{dp(1, t)}{dt} = -(\alpha + \beta) p(1, t) + \beta p(2, t) \quad (128)$$

$$\frac{dp(0, t)}{dt} = \beta p(1, t) \quad (129)$$

with the initial conditions

$$p(m_0, 0) = 1, \quad p(m, 0) = 0 \quad (m \neq m_0) \quad (130)$$

The analytical solution of $p(m, t)$ is known (Goel and Richter-Dyn 1974) and given by

$$p(m, t) = \rho^{(m-m_0)/2} e^{-(\alpha+\beta)t} [I_{m-m_0}(\omega t) - I_{m+m_0}(\omega t)] \quad (m \geq 1) \quad (131)$$

The rate of absorption $u(t)$ at $m = 0$ is

$$u(t) = \frac{dp(0, t)}{dt} = \beta p(1, t) = m_0 \rho^{-m_0/2} t^{-1} e^{-(\alpha+\beta)t} I_{m_0}(\omega t) \quad (132)$$

and therefore, the probability of the cap eventually reaching $m = 0$ is

$$\lim_{t \rightarrow \infty} p(0, t) = \int_0^{\infty} u(t) dt \quad (133)$$

$$= m_0 \rho^{-m_0/2} \int_0^{\infty} t^{-1} e^{-(\alpha+\beta)t} I_{m_0}(\omega t) dt \quad (134)$$

$$= m_0 \rho^{-m_0/2} \int_0^{\infty} t^{-1} I_{m_0}(t) e^{-\frac{\alpha+\beta}{2\sqrt{\alpha\beta}}t} dt \quad (135)$$

The integral term of (135) can be viewed as value of the Laplace transform of $t^{-1} I_{m_0}(t)$ at $s = (\alpha + \beta)/(2\sqrt{\alpha\beta})$. Since the Laplace transform of $I_{m_0}(t)$ is $(\sqrt{s^2 - 1})^{-1}$

$(s + \sqrt{s^2 - 1})^{-m_0}$, one obtains

$$\lim_{t \rightarrow \infty} p(0, t) = m_0 \rho^{-m_0/2} \int_{\frac{\alpha+\beta}{2\sqrt{\alpha\beta}}}^{\infty} (\sqrt{s^2 - 1})^{-1} (s + \sqrt{s^2 - 1})^{-m_0} ds \quad (136)$$

$$= -\rho^{-m_0/2} \int_{\frac{\alpha+\beta}{2\sqrt{\alpha\beta}}}^{\infty} d \left((s + \sqrt{s^2 - 1})^{-m_0} \right) \quad (137)$$

$$= \left(\sqrt{\frac{\beta}{\alpha}} \right)^{m_0} \left\{ \frac{1}{2} \left| \sqrt{\frac{\alpha}{\beta}} + \sqrt{\frac{\beta}{\alpha}} \right| + \frac{1}{2} \left| \sqrt{\frac{\alpha}{\beta}} - \sqrt{\frac{\beta}{\alpha}} \right| \right\}^{-m_0} \quad (138)$$

That is,

$$\lim_{t \rightarrow \infty} p(0, t) = \begin{cases} 1, & \text{if } \alpha \leq \beta \\ (\beta/\alpha)^{m_0}, & \text{if } \alpha > \beta \end{cases} \quad (139)$$

Therefore, the cap will disappear with probability one when the on-rate of A is less than or equal to its off-rate. Otherwise, it has a probability of $1 - (\beta/\alpha)^{m_0}$ of never reaching $m = 0$. The first case is equivalent to the well-known result for random walks in 1D.

We next calculate the mean and variance of the first passage time to the origin when $\alpha < \beta$, in which case the walker visits $m = 0$ with probability one. By definition, the probability density of the first passage time $g(t)$ is equal to the absorption rate $u(t)$ for this model, i.e.,

$$g(t) = \frac{dp(0, t)}{dt} = m_0 \rho^{m_0/2} t^{-1} e^{-(\alpha+\beta)t} I_{m_0}(\omega t) \quad (140)$$

The mean first passage time is

$$\begin{aligned} \langle t \rangle &= \int_0^{\infty} t g(t) dt \\ &= m_0 \rho^{-m_0/2} \int_0^{\infty} I_{m_0}(\omega t) e^{-(\alpha+\beta)t} dt \\ &= m_0 \rho^{-m_0/2} F(\alpha + \beta) \\ &= m_0/(\beta - \alpha) \end{aligned} \quad (141)$$

where $F(s)$ is the Laplace transform of $I_{m_0}(\omega t)$. Thus the mean first passage time can be understood as the cap size divided by the net disassociation rate. The second

moment is

$$\begin{aligned}
 \langle t^2 \rangle &= \int_0^{\infty} t^2 g(t) dt \\
 &= m_0 \rho^{-m_0/2} \int_0^{\infty} t I_{m_0}(\omega t) e^{-(\alpha+\beta)t} dt \\
 &= -m_0 \rho^{-m_0/2} F'(\alpha + \beta) \\
 &= \frac{m_0^2}{(\beta - \alpha)^2} + \frac{m_0(\beta + \alpha)}{(\beta - \alpha)^3}
 \end{aligned} \tag{142}$$

where $F'(s)$ is derivative of the Laplace transform of $I_{m_0}(\omega t)$. Therefore the variance of the first passage time is

$$\langle t^2 \rangle - \langle t \rangle^2 = \frac{m_0(\beta + \alpha)}{(\beta - \alpha)^3} \tag{143}$$

It should be noted that this diverges as $\beta \rightarrow \alpha$. In the following section we show that this variance is important for an alternate route to the long-time filament length diffusion coefficient.

3.5 An alternate route to the stationary drift and diffusion rates

Since changes in the lengths of the A- and B-segments are mutually exclusive processes, a coarser description of the evolution of a filament is as a random walk with two-states—one corresponding to the B-segment and one to the A-cap—with an embedded Markov process that switches between the states. One state transition is from a cap-free B-segment to the capped state, whereas the other transition is the reverse of this. The asymptotic behavior of a two-state random walk in continuous time and space has been studied by Weiss (1976). In that model a diffusing species can switch between two states having different diffusion constants. The probability density for a single sojourn in state i is denoted as $\psi_i(t)$ ($i = 1, 2$). The dynamics of molecules in these two states are characterized by their average speed v_i and diffusion constant D_i . Assuming that the mean and variance with respect to $\psi_i(t)$, $\langle t \rangle_i$ and σ_i^2 , are both finite, Weiss obtained the asymptotic convective speed and effective diffusion rate constants as

$$\bar{v} = \frac{\langle t \rangle_1}{\langle t \rangle} v_1 + \frac{\langle t \rangle_2}{\langle t \rangle} v_2 \tag{144}$$

$$\begin{aligned}
 D_{eff} &= \frac{\langle t \rangle_1}{\langle t \rangle} D_1 + \frac{\langle t \rangle_2}{\langle t \rangle} D_2 \\
 &\quad + \frac{1}{2}(v_1 - v_2)^2 \left[\left(\frac{\langle t \rangle_2}{\langle t \rangle} \right)^2 \sigma_1^2 + \left(\frac{\langle t \rangle_1}{\langle t \rangle} \right)^2 \sigma_2^2 \right] / \langle t \rangle
 \end{aligned} \tag{145}$$

where $\langle t \rangle = \langle t \rangle_1 + \langle t \rangle_2$.

In the present context, the uncapped state is terminated upon addition of the first G-ATP, which is a Poisson process with parameter α because the monomer concentration is constant. Therefore the probability density for the time that a filament remains uncapped is exponential with constant α . On the other hand, the dynamics for transitions from the capped state with an initial cap size of one is identical to the dynamics of the random walk beginning at $m = 1$ with the absorbing boundary condition at $m = 0$, as described by Eq. (128). At this level of description the filament sojourns in two distinct states: the uncapped and the capped state, and the probability density of the sojourn time in the uncapped state is

$$g_u(t) = e^{-\alpha t} \quad (146)$$

and that in the capped state is as in Eq. (140) with $n_0 = 1$, i.e.,

$$g_c(t) = \sqrt{\alpha/\beta} t^{-1} e^{-(\alpha+\beta)t} I_1(2t\sqrt{\alpha\beta}) \quad (147)$$

Therefore, the mean and variance of the sojourn times in the two states are

$$m_u = \frac{1}{\alpha}, \quad \sigma_u^2 = \frac{1}{\alpha^2} \quad (148)$$

$$m_c = \frac{1}{\beta - \alpha}, \quad \sigma_c^2 = \frac{\beta + \alpha}{(\beta - \alpha)^3} \quad (149)$$

Note that if the maximal cap size $m_{max} = 1$, as applies if the ‘side-walk’ is binding to a receptor, then the mean time in the capped state is $1/\beta$, which differs from $m_c = 1/(\beta - \alpha)$ when the cap size can be of any integer.

When $\alpha < \beta$, the occasional capping of a filament prevents the core from (de)polymerizing – thus the length of the core is unchanged – whereas in the absence of a cap, the core undergoes a biased random walk. Thus the elongation rates and diffusion rates for the B-core in these states are

$$j_u = r - s, \quad D_u = (r + s)/2 \quad (150)$$

$$j_c = 0, \quad D_c = 0 \quad (151)$$

Using Eqs. (144), (145) one can obtain the same asymptotic elongation and diffusion constants as in Eqs. (98) and (99). Therefore the effective elongation rate is equal to the elongation rate when the cap is absent times the proportion of time that the cap is absent. The effective diffusion coefficient has two sources: first, the stochastic Poisson process of monomer disassociation when the cap is absent, and second, the stochastic capping. Both the mean and variance of the cap life time determine the diffusion rate constant. However our treatment of a generic two-state filament model also provides the transient behavior of the mean and variance of filament lengths, which is important for understanding the approach to the stationary values.

4 Applications to actin filament dynamics

The previous results apply to general polymerization reactions, but can be specialized for actin filaments. In this section we analyze some actin-specific problems, that of fragmentation and that of hydrolysis of ATP.

4.1 The role of fragmentation at the ATP-ADP interface

Spontaneous filament fragmentation and/or protein-regulated severing can also contribute to the large length fluctuations, and where in a filament they occur is known to depend on the actin-bound nucleotide type. It is known that ADF/cofilin (AC) bind preferentially to ADP-containing monomers in a filament, and that filaments tend to break at AC-free monomers between neighboring ACs (De La Cruz 2009). It is also known that the fragmentation rate increases at low AC concentrations but decreases at high AC concentration, which indicates that the filament is stabilized at high AC concentrations (De La Cruz 2009). In the following we assume that fragmentation occurs only at the interface between monomers containing ATP and ADP. Thus the following analysis can be regarded as a first approximation to the dynamics at high AC concentrations, when the most probable fragmentation site is at the ATP-ADP interface, because the ADP-Pi state is ignored here. As in previous sections, we calculate the mean and variance of the lifetime of the cap in order to obtain the large-time behavior of the filament length fluctuations.

The one-step changes in the filament remain as described in the previous sections, but now the cap can also be removed from the filament at a rate k_f . Let $c(m, t)$ denote the probability of a filament with a cap of size m at time t , which is given by $c(m, t) = \sum_n p(m, n, t)$ and satisfies

$$\frac{dc(0, t)}{dt} = -\alpha c(0, t) + \beta c(1, t) + k_f \sum_{m=1}^{\infty} c(m, t) \quad (152)$$

$$\frac{dc(m, t)}{dt} = \alpha c(m-1, t) - R c(m, t) + \beta c(m+1, t) \quad (m \geq 1) \quad (153)$$

where $\alpha = k_T^+ c$, $\beta = k_T^-$ are the on- and off-rate of G-ATP and $R \equiv \alpha + \beta + k_f$. The steady state of the cap size distribution is found to be

$$c_m^\infty = \lim_{t \rightarrow \infty} c(m, t) = (1-x) x^m \quad (154)$$

where

$$x = \frac{R - \sqrt{R^2 - 4\alpha\beta}}{2\beta} \quad (155)$$

Thus the probability of a filament being bare is $1-x$, whereas it is capped with probability x . Interestingly, the steady-state cap size with fragmentation is a geometric

distribution as in the case without fragmentation. Note that at equilibrium the right hand side of Eq. (153) leads to a linear recurrence relation for the c_m^∞ 's, which provides an alternate route to the steady-state distribution.

To obtain the survival time of a cap, we denote the probability of the cap being of size m at time as $s(m, t)$ and suppose the initial size of the cap is m_0 . As in the previous section, we have to solve the following ODE

$$\frac{ds(m, t)}{dt} = \alpha s(m - 1, t) - R s(m, t) + \beta s(m + 1, t) \tag{156}$$

$$\frac{ds(1, t)}{dt} = -R s(1, t) + \beta s(2, t) \tag{157}$$

$$\frac{ds(0, t)}{dt} = \beta s(1, t) + k_f \sum_{m=1}^{\infty} s(m, t) \tag{158}$$

with an absorbing boundary condition and with the initial condition

$$s(m_0, 0) = 1, \quad s(m, 0) = 0 \quad \text{when } m \neq m_0$$

By applying the method of generating functions, one can write the solution in terms of modified Bessel functions as follows

$$s(m, t) = e^{-R t} \left(\sqrt{\frac{\alpha}{\beta}} \right)^{m-m_0} \left(I_{m-m_0} \left(2\sqrt{\alpha\beta t} \right) - I_{m+m_0} \left(2\sqrt{\alpha\beta t} \right) \right) \tag{159}$$

As in the previous section, the probability density of the survival time for a cap with initial size $m_0 = 1$ equals the absorption rate at the boundary $m = 0$, i.e.

$$g(t) = \frac{ds(0, t)}{dt} = \beta s(1, t) + k_f \sum_{m=1}^{\infty} s(m, t) \tag{160}$$

$$\begin{aligned} &= \left(\beta + \frac{\beta}{\alpha} k_f \right) I_0 e^{-R t} \\ &+ k_f \sqrt{\frac{\beta}{\alpha}} I_1 e^{-R t} - \beta I_2 e^{-R t} \\ &+ k_f \left(1 - \frac{\beta}{\alpha} \right) \sum_{m=0}^{\infty} \left[\left(\sqrt{\frac{\alpha}{\beta}} \right)^m I_m e^{-R t} \right] \end{aligned} \tag{161}$$

It is easy to check that

$$\begin{aligned} 1 &= \int_0^{\infty} g(t) dt \\ &= \left(\beta + \frac{\beta}{\alpha} k_f \right) F_0(R) \end{aligned}$$

$$\begin{aligned}
 &+k_f\sqrt{\frac{\beta}{\alpha}} F_1(R) - \beta F_2(R) \\
 &+k_f\left(1 - \frac{\beta}{\alpha}\right) \sum_{m=0}^{\infty} \left[\left(\sqrt{\frac{\alpha}{\beta}}\right)^m F_m(R) \right]
 \end{aligned} \tag{162}$$

where $F_m(s)$ is the Laplace transform of the modified Bessel functions $I_m(\omega t)$. This indicates that the cap eventually disappears, which is different from the earlier case in which this integral could be less than one in the absence of fragmentation and $\alpha > \beta$. Fragmentation prevents unbounded growth of the cap even for $\alpha > \beta$.

One can also calculate the first and second moments of $g(t)$, and one finds that

$$\begin{aligned}
 \int_0^{\infty} t \cdot g(t) dt &= -\left(\beta + \frac{\beta}{\alpha} k_f\right) F'_0(R) \\
 &\quad -k_f\sqrt{\frac{\beta}{\alpha}} F'_1(R) + \beta F'_2(R) \\
 &\quad -k_f\left(1 - \frac{\beta}{\alpha}\right) \sum_{m=0}^{\infty} \left[\left(\sqrt{\frac{\alpha}{\beta}}\right)^m F'_m(R) \right] \\
 &= \frac{1}{\alpha} \frac{x}{1-x}
 \end{aligned} \tag{163}$$

$$\begin{aligned}
 \int_0^{\infty} t^2 \cdot g(t) dt &= \left(\beta + \frac{\beta}{\alpha} k_f\right) F''_0(R) \\
 &\quad +k_f\sqrt{\frac{\beta}{\alpha}} F''_1(R) - \beta F''_2(R) \\
 &\quad +k_f\left(1 - \frac{\beta}{\alpha}\right) \sum_{m=0}^{\infty} \left[\left(\sqrt{\frac{\alpha}{\beta}}\right)^m F''_m(R) \right]
 \end{aligned} \tag{164}$$

where x is defined in (154), and F'_m, F''_m are the first and second derivatives of F_m , respectively. Therefore, the mean and variance of the survival time of caps are

$$\langle t \rangle = \int_0^{\infty} t \cdot g(t) dt = \frac{1}{\alpha} \frac{x}{1-x} \tag{165}$$

$$\begin{aligned}
 \langle t^2 \rangle - \langle t \rangle^2 &= \int_0^{\infty} (t - \langle t \rangle)^2 \cdot g(t) dt \\
 &= \frac{R}{4\alpha^2 k_f^2} \frac{(R - 2\alpha - Q)^2}{Q}
 \end{aligned} \tag{166}$$

where

$$Q = \sqrt{R^2 - 4\alpha\beta} \quad (167)$$

Just as in the previous case, a filament subject to fragmentation sojourns in two states: the uncapped state and capped state. The mean and variance of sojourn time in these states are

$$m_u = \frac{1}{\alpha}, \quad \sigma_u^2 = \frac{1}{\alpha^2} \quad (168)$$

$$m_c = \frac{1}{\alpha} \frac{x}{1-x}, \quad \sigma_c^2 = \frac{R}{4\alpha^2 k_f^2} \frac{(R - 2\alpha - Q)^2}{Q} \quad (169)$$

The elongation rates and diffusion coefficients for these two states are

$$j_u = -k_D^-, \quad D_u = k_D^-/2, \quad j_c = 0, \quad D_c = 0 \quad (170)$$

According to the results of Weiss' two-state random walk (see Eqs. (144) and (145)), the asymptotic expression for the mean elongation and effective length diffusion coefficient are

$$j = -s \frac{2\beta - R + Q}{2\beta} \quad (171)$$

$$D = s \frac{2\beta - R + Q}{4\beta} + \frac{(2\beta - R + Q)(R - Q)s^2}{4\beta^2 Q} \quad (172)$$

where $\alpha = k_T^+ c$, $\beta = k_T^-$, $s = k_D^-$ and R, Q are defined in (167).

The dependence of the elongation rate and length diffusion coefficient on the G-ATP concentration and fragmentation rates is shown in Fig. 5. We note that with fragmentation the net elongation rate is negative at all monomer concentrations, because removal of the caps exposes the ADP-core—which shrinks rapidly. In Fig. 5, we also observe that the higher the fragmentation rate, the higher the net shrinking rate filaments, due to the increased frequency of exposing the ADP-subunits. When the fragmentation increases, the diffusion rate constant curve smooths out in the neighborhood of the critical concentration. In the presence of fragmentation, the filament exposes ADP-core at all monomer concentrations. However, without fragmentation, when $\alpha > \beta$, the addition of G-ATP is faster than loss, and the ADP-core will rarely be exposed at large times. In short, the size of the discontinuity of the diffusion coefficient depends on the frequency at which the ADP core is exposed during polymerization. Moreover, the maximal diffusion coefficient decreases with increasing fragmentation.

4.2 Filament length fluctuation with ATP hydrolysis

In the previous section we investigated the dynamic and asymptotic behavior of actin filament length fluctuations, when the filament is composed of non-overlapping ADP

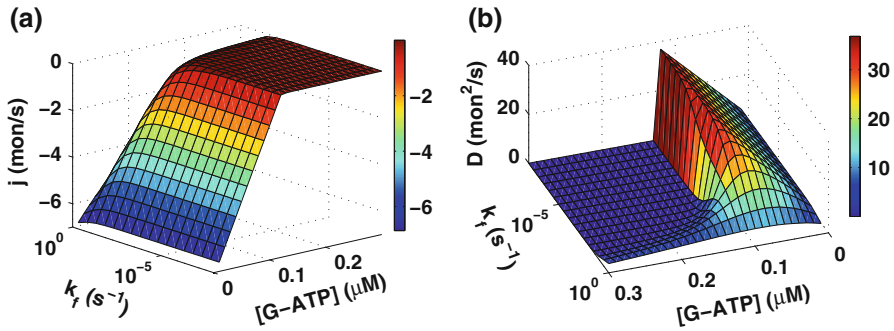


Fig. 5 The asymptotic elongation rate (a) and the diffusion constant (b) versus the G-ATP concentration and the fragmentation rates. The kinetic constants used in the simulations are from Vavylonis et al. (2005): $k_T^+ = 11.6 \mu\text{Ms}^{-1}$, $k_T^- = 1.4\text{s}^{-1}$, $k_D = 7.2\text{s}^{-1}$

and ATP segments and no hydrolysis of ATP is considered. In this section we study the dynamics of the filament lengths when vectorial ATP hydrolysis occurs, i.e., hydrolysis occurs at one point in the filament, which defines the junction between the two segments. The rate of hydrolysis (or conversion of ATP to ADP) is h . The master equation for $p(m, n, t)$ then becomes

$$\frac{dp(0, n, t)}{dt} = -\alpha p(0, n, t) + \beta p(1, n, t) - (r + s) p(0, n, t) + r p(0, n - 1, t) + s p(0, n + 1, t) + h p(1, n - 1, t) \quad (173)$$

$$\frac{dp(m, n, t)}{dt} = \alpha p(m - 1, n, t) + \beta p(m + 1, n, t) - (\alpha + \beta) p(m, n, t) + h p(m + 1, n - 1, t) - h p(m, n, t), \quad m \geq 1 \quad (174)$$

where as before m, n denote the size of the ATP- and ADP-segments, and $\alpha = k_T^+ c$, $\beta = k_T^-$, $s = k_D^-$, and $r = 0$.

Similarly, we define the following quantities

$$P_m(t) = \sum_{n=-\infty}^{\infty} p(m, n, t), \quad L_m(t) = \sum_{n=-\infty}^{\infty} n p(m, n, t)$$

$$M_y(t) = \sum_{m=0}^{\infty} L_m(t), \quad M(t) = \sum_{n=-\infty}^{\infty} \sum_{m=0}^{\infty} (m + n) p(m, n, t)$$

$$V(t) = \sum_{n=-\infty}^{\infty} \sum_{m=0}^{\infty} (m + n)^2 p(m, n, t), \quad \sigma^2(t) = V(t) - M^2(t)$$

where $M(t)$ and $\sigma^2(t)$ are the mean and variance of filament lengths, respectively. From Eqs. (174), (173), we have

$$\begin{cases} \frac{dP_m(t)}{dt} = \alpha P_{m-1}(t) + (\beta + h) P_{m+1}(t) - (\alpha + \beta + h) P_m(t) \\ \frac{dP_0(t)}{dt} = -\alpha P_0(t) + (\beta + h) P_1(t) \end{cases} \tag{175}$$

$$\begin{cases} \frac{dL_m(t)}{dt} = \alpha L_{m-1}(t) + (\beta + h) L_{m+1}(t) - (\alpha + \beta + h) L_m(t) + h P_{m+1} \\ \frac{dL_0(t)}{dt} = -\alpha L_0(t) + (\beta + h) L_1(t) + (r - s) P_0(t) + h P_1 \end{cases} \tag{176}$$

We assume that the polymer contains l_0 ADP-bound monomers initially, and thus the initial condition is

$$P_0(0) = 1, P_m(0) = 0 \text{ for } m \geq 1 \tag{177}$$

$$L_0(0) = l_0, L_m(0) = 0 \text{ for } m \geq 1 \tag{178}$$

The solution for $P_m(t)$ is similar to that given in Eq. (42),

$$P_m(t) = e^{-(\alpha+\beta+h)t} \left(\rho_h^{m/2} I_m(\omega_h t) + \rho_h^{\frac{m-1}{2}} I_{m+1}(\omega_h t) + (1 - \rho_h) \sum_{k=2}^{\infty} \rho_h^{\frac{m-k}{2}} I_{m+k}(\omega_h t) \right) \tag{179}$$

where $\rho_h = \alpha/(\beta + h)$, $\omega_h = 2\sqrt{\alpha(\beta + h)}$. We also find that $L_m(t)$ is

$$L_m(t) = L_m^0(t) + ht P_{m+1}(t) + \delta_m(t) \tag{180}$$

where

$$L_m^0(t) = l_0 P_m(t) - \frac{s - r}{\beta + h} e^{-(\alpha+\beta+h)t} \left(\rho_h^{\frac{m-1}{2}} I_{m+1}(\omega_h t) + 2\rho_h \sum_{k=2}^{\infty} \rho_h^{\frac{m-k}{2}} I_{m+k}(\omega_h t) + (1 - \rho_h) \sum_{k=2}^{\infty} \rho_h^{\frac{m-k}{2}} k I_{m+k}(\omega_h t) \right)$$

and

$$\begin{aligned} \delta_m(t) &= h \int_0^t P_m(t - \tau) \tau dP_0(\tau) \\ &= -\rho_h^{1/2} \int_0^t P_0(t - \tau) e^{-(\alpha+\beta+h)\tau} I_1 \left(2\sqrt{\alpha(\beta + h)} \tau \right) d\tau \end{aligned} \tag{181}$$

Moreover, when $\alpha < \beta + h$

$$\lim_{t \rightarrow \infty} \delta_m(t) = -\frac{h}{\beta + h} \rho_h^{m+1}$$

and when $\alpha > \beta + h$

$$\lim_{t \rightarrow \infty} \delta_m(t) = 0$$

The evolution equations for the mean and variance can be derived from Eqs. (173), (174), and are given by

$$\begin{aligned} \frac{dM_y(t)}{dt} &= h - (s + h - r) P_0 \\ \frac{d\sigma_y^2(t)}{dt} &= h + (r + s - h) P_0 + 2(s + h - r)(M_y P_0 - L_0) \\ \frac{dM(t)}{dt} &= \alpha - \beta + (\beta + r - s) P_0 \\ \frac{d\sigma^2(t)}{dt} &= (\alpha + \beta) + (r + s - \beta) P_0 - 2(\beta + r - s)(M P_0 - L_0) \end{aligned} \quad (182)$$

So

$$\begin{aligned} M(t) &= \frac{\beta + h}{s + h - r} l_0 + \left(\alpha - \beta - \frac{s - r - \beta}{s + h - r} h \right) t + \frac{s - r - \beta}{s + h - r} M_y \\ M_y(t) &= \sum_{m=0}^{\infty} L_m(t) \\ &= l_0 + (h - (s + h - r) P_0) t \\ &\quad - \frac{s + h - r}{\beta + h} \frac{1}{1 - \rho_h} \left(\frac{1 + \rho_h}{1 - \rho_h} P_0 - 1 \right) \\ &\quad + \frac{s + h - r}{\beta + h} e^{-(\alpha + \beta + h)t} \left(\frac{2\rho_h}{(1 - \rho_h)^2} I_0 + \frac{1 + \rho_h}{(1 - \rho_h)^2} \rho_h^{1/2} I_1 \right) \end{aligned} \quad (183)$$

Therefore,

$$\begin{aligned} M(t) &= l_0 - \frac{s - r - \beta}{\beta + h} \frac{1}{1 - \rho_h} \left(\frac{1 + \rho_h}{1 - \rho_h} P_0 - 1 \right) \\ &\quad + (\alpha - \beta - (s - r - \beta) P_0) t \\ &\quad + \frac{s - r - \beta}{\beta + h} e^{-(\alpha + \beta + h)t} \left(\frac{2\rho_h}{(1 - \rho_h)^2} I_0 + \frac{1 + \rho_h}{(1 - \rho_h)^2} \rho_h^{1/2} I_1 \right) \end{aligned} \quad (184)$$

According to (180),

$$L_0(t) = l_0 P_0 - \frac{s-r}{\beta+h} \frac{2\rho_h}{1-\rho_h} P_0 + (r-s)(1-\rho_h) P_0 t + h P_1 t + \delta_0 + \frac{s-r}{\beta+h} e^{-(\alpha+\beta+h)t} \left(\frac{2\rho_h}{1-\rho_h} I_0 + \frac{1+\rho_h}{1-\rho_h} \rho_h^{1/2} I_1 \right) \tag{185}$$

and from Eqs. (179), (184) and (185) we obtain the transient dynamics of the elongation rate and diffusion constant

$$j(t) = \alpha - \beta + (\beta + r - s) P_0 \tag{186}$$

$$D(t) = \frac{\alpha + \beta}{2} + \frac{r + s - \beta}{2} P_0 - (\beta + r - s)(M P_0 - L_0) \tag{187}$$

They have the following asymptotic behavior:

Case I: $\alpha < \beta + h$ At large times, one has

$$\lim_{t \rightarrow \infty} j(t) = \frac{h\alpha}{\beta+h} + (r-s) \left(1 - \frac{\alpha}{\beta+h} \right) \tag{188}$$

$$\lim_{t \rightarrow \infty} D(t) = \frac{\alpha h}{2(\beta+h)} - \frac{\alpha h(r-s)}{(\beta+h)^2} + \frac{r+s}{2} \left(1 - \frac{\alpha}{\beta+h} \right) + \frac{\alpha(r-s)^2}{(\beta+h)^2} \tag{189}$$

Since $\alpha = k_T^+ c$, $\beta = k_T^-$, $s = k_D^-$, and $r = 0$ for an actin filament, we have

$$\lim_{t \rightarrow \infty} j(t) = \frac{k_T^+ c h}{k_T^- + h} - \left(1 - \frac{k_T^+ c}{k_T^- + h} \right) k_D^- \tag{190}$$

$$\lim_{t \rightarrow \infty} D(t) = \frac{h}{k_T^- + h} \frac{k_T^+ c}{2} + \left(1 + \frac{h - k_T^-}{h + k_T^-} \frac{k_T^+ c}{k_T^- + h} \right) \frac{k_D^-}{2} + \frac{k_T^+ c}{k_T^- + h} \frac{(k_D^-)^2}{k_T^- + h} \tag{191}$$

This corresponds to the bounded growth Phase I and intermediate Phase II in Ranjith et al. (2009), where the ATP-cap length is finite. According to Eq. (190), the critical concentration of G-ATP at which the net filament elongation vanishes is

$$c_{crit} = \frac{k_T^- + h}{k_T^+} \frac{k_D^-}{k_D^- + h} = \frac{k_T^-}{k_T^+} \frac{1 + h/k_T^-}{1 + h/k_D^-} \tag{192}$$

which is larger than the case without hydrolysis ($h = 0$) because $k_T^- < k_D^-$. The transition concentration of Phase I and II in Ranjith et al. (2009) is exactly the critical concentration as defined in (192). In Ranjith et al. (2009), the filament length

distribution in Phase I approaches to a finite steady state, which has zero elongation rate and diffusion coefficient. However, we consider the stable elongation and length fluctuation before the filament length reaches zero. This is why we have values for elongation and diffusion which differ from those in [Ranjith et al. \(2009\)](#).

Case II: $\alpha > \beta + h$ In this case

$$\lim_{t \rightarrow \infty} P_0(t) = 0, \quad \lim_{t \rightarrow \infty} M(t)P_0(t) = 0, \quad \lim_{t \rightarrow \infty} L_0(t) = 0$$

and therefore at large times

$$\lim_{t \rightarrow \infty} j(t) = k_T^+ c - k_T^-, \quad \lim_{t \rightarrow \infty} D(t) = (k_T^+ c + k_T^-) / 2 \tag{193}$$

Thus the cap size expands linearly at large times, which permanently caps the ADP-core. This corresponds to the rapidly growing Phase III of filament polymerization with hydrolysis in [Ranjith et al. \(2009\)](#).

Case III: $\alpha = \beta + h$ Here we find that the asymptotic behavior of the elongation rate and diffusion constant are

$$\lim_{t \rightarrow \infty} j(t) = h \tag{194}$$

$$\lim_{t \rightarrow \infty} D(t) = h/2 + k_D^- + \frac{k_T^- - k_D^-}{k_T^- + h} \frac{h}{\pi} + \frac{(k_T^- - k_D^-)^2}{k_T^- + h} \left(1 - \frac{2}{\pi}\right) \tag{195}$$

This is the transition case between a finite and infinite the cap. For the three cases, when h approaches zero, the elongation rate and diffusion coefficient approaches to those derived in the absence of hydrolysis.

The dependence of the asymptotic elongation rate and diffusion coefficient on the G-ATP concentration and the hydrolysis rate is depicted in [Fig. 6](#). The elongation rates are continuous for all G-ATP concentrations, whereas the diffusion coefficient is discontinuous at $c = (k_T^- + h) / k_T^+$. When $\alpha > \beta + h$, the addition rate of G-ATP exceeds the decay rate, and thus the filament end is capped by ATP on average. The filament length fluctuations under this condition are due to the kinetics of G-ATP. When $\alpha < \beta + h$, the filament occasionally loses its ATP-cap and exposes the ADP core, which has different kinetics from that of G-ATP. The combined dynamics of G-ADP and G-ATP give rise to large filament length fluctuations. The maximal diffusion coefficient occurs as α approaches $\beta + h$ from below, i.e. as $c \rightarrow (k_T^- + h) / k_T^+$,

$$D_{max} = \frac{h}{2} + \frac{k_D^- + h}{k_T^- + h} k_D^-$$

which agrees with previous results in [Stukalin and Kolomeisky \(2006\)](#), [Ranjith et al. \(2009\)](#). From [\(191\)](#) and [\(195\)](#), the diffusion constant drops at the discontinuity

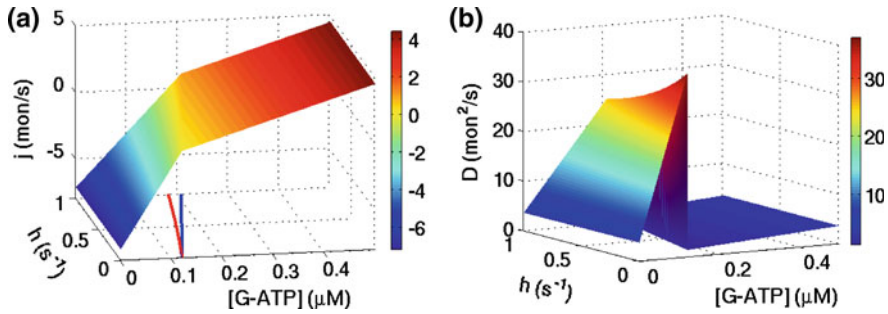
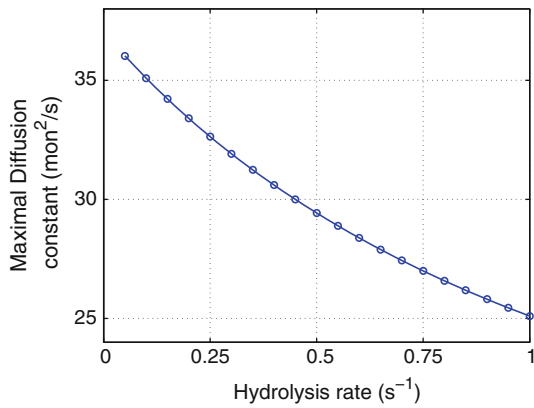


Fig. 6 The asymptotic elongation rate (a) and diffusion constant (b) versus the G-ATP concentration and the hydrolysis rate. The kinetic constants used in the simulations are from Vavylonis et al. (2005): $k_T^+ = 11.6 \mu\text{Ms}^{-1}$, $k_T^- = 1.4 \text{s}^{-1}$, $k_D^- = 7.2 \text{s}^{-1}$. The leftmost line in (a) represents the critical concentration of G-ATP as in (192), whereas the rightmost line depicts the concentrations, $c = (k_T^- + h)/k_T^+$, at which the elongation rate curve changes slope

Fig. 7 A cross-section of Fig. 6b showing the maximum diffusion coefficient as a function of the hydrolysis rate



concentration

$$\Delta D = (k_D^- - k_T^-) \left(1 + \frac{k_D^-}{k_T^- + h} \right) \tag{196}$$

Moreover, the higher the hydrolysis rate the lower the maximal diffusion rate constant is, and the monotone relationship between these two is shown in Fig. 7. The elongation rate and diffusion rate constant with two different hydrolysis rates ($h = 0, 0.3$) are compared in Fig. 8. At the same G-ATP concentration, hydrolysis slows the elongation rate. It also increases the critical concentration. When the G-ATP level is less than k_T^-/k_T^+ , the fluctuations without hydrolysis are higher than with it. However, the fluctuation is larger with hydrolysis when the level of G-ATP is between k_T^-/k_T^+ and $(k_T^- + h)/k_T^+$. Moreover, at the discontinuity concentration the diffusion constant drop is larger in the presence of hydrolysis as in Fig. 8.

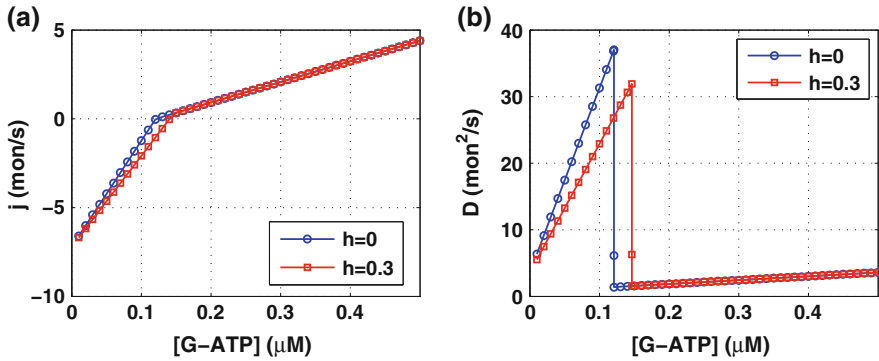


Fig. 8 The asymptotic elongation rate (a) and diffusion constant (b) versus the G-ATP concentration for two hydrolysis rates, using the kinetic constants in Fig. 6. Note that vectorial hydrolysis reduces the diffusion constant fluctuation near the critical concentration

4.3 The dynamics of the cap in the presence of hydrolysis

In the presence of vectorial hydrolysis, the probability of a cap of length m , $c(m, t)$, evolves according to

$$\frac{dc(0, t)}{dt} = -\alpha c(0, t) + (\beta + h) c(1, t) \tag{197}$$

$$\begin{aligned} \frac{dc(m, t)}{dt} = & \alpha c(m - 1, t) - (\alpha + \beta + h) c(m, t) \\ & + (\beta + h) c(m + 1, t) \quad (m \geq 1) \end{aligned} \tag{198}$$

The transient dynamics of the mean and variance of cap lengths are given by

$$m_c(t) = (\beta + h)(\rho_h - 1)t + (\beta + h) \int_0^t P_0(\tau) d\tau \tag{199}$$

$$\begin{aligned} \sigma_c^2(t) = & (\beta + h)(1 + \rho_h)t + 2(\beta + h)^2(1 - \rho_h) \int_0^t P_0(\tau) \tau d\tau \\ & - (\beta + h) \int_0^t P_0(\tau) d\tau - (\beta + h)^2 \left(\int_0^t P_0(\tau) d\tau \right)^2 \end{aligned} \tag{200}$$

where $P_0(t)$ is defined in (179).

From (175) we obtain the following variables quantifying the convergence of $P_m(t)$'s to their steady state: when $\alpha < \beta + h$

$$P_m^\infty = \lim_{t \rightarrow \infty} P_m(t) = (1 - \rho_h) \rho_h^m \tag{201}$$

$$\int_0^{\infty} (P_m(\tau) - P_m^{\infty}) d\tau = \frac{(m+1)\rho_h^{m+1} - m\rho_h^m}{(\beta+h)(1-\rho_h)} \quad (202)$$

$$\int_0^{\infty} (P_m(\tau) - P_m^{\infty}) \tau d\tau = \frac{\rho_h^m}{(\beta+h)^2(1-\rho_h)} \times \left[\frac{\rho_h}{(1-\rho_h)^2} - \frac{m(m+1)}{2} \right] \quad (203)$$

and when $\alpha > \beta + h$

$$P_m^{\infty} = 0 \quad (204)$$

$$\int_0^{\infty} P_m(\tau) d\tau = \frac{1}{(\beta+h)(\rho_h-1)} \quad (205)$$

$$\int_0^{\infty} P_m(\tau) \tau d\tau = \frac{\rho_h}{(\beta+h)^2(\rho_h-1)^3} + \frac{m}{(\beta+h)^2(\rho_h-1)^2} \quad (206)$$

Therefore, for $\alpha < \beta + h$, the mean and variance approach

$$\lim_{t \rightarrow \infty} m_c(t) = \frac{\rho_h}{1-\rho_h}, \quad \lim_{t \rightarrow \infty} \sigma_c^2(t) = \frac{\rho_h}{(1-\rho_h)^2} \quad (207)$$

whereas for $\alpha > \beta + h$

$$m_c(t) - (\alpha - (\beta + h))t \rightarrow \frac{1}{\rho_h - 1}, \quad \text{as } t \rightarrow \infty \quad (208)$$

$$\sigma_c^2(t) - (\alpha + \beta + h)t \rightarrow -\frac{3\rho_h}{(\rho_h - 1)^2}, \quad \text{as } t \rightarrow \infty \quad (209)$$

Thus we conclude that when $\alpha < \beta + h$ the cap size approaches a geometric distribution $P_m(\infty) = \rho_h^m(1-\rho_h)$. When $\alpha > \beta + h$, the cap dynamics resembles a convection-diffusion process with drift velocity $v = \alpha - (\beta + h)F$, and diffusion constant $D = (\alpha + \beta + h)/2$.

A typical filament devoid of an ATP cap goes through the following polymerization cycle: it releases its G-ADP, which is followed by a period in which it has an ATP cap. When the G-ADP core is exposed it shrinks rapidly. When capped with ATP, the cap size fluctuates while the ADP portion steadily elongates due to continuous ATP hydrolysis. When $\alpha > \beta + h$, the ATP cap will grow indefinitely and simultaneously the length of the ADP portion increases. Snapshots of the filament length fluctuations at various G-ATP concentrations are shown in Fig. 9, where (a) and (b) correspond to $\alpha < \beta + h$, (c) to $\alpha = \beta + h$ and (d) to $\alpha > \beta + h$. The results show that the changes of the total filament length are controlled by changes of the ADP core, which increases when the ATP cap is present and decreases when the cap is absent. This qualitatively

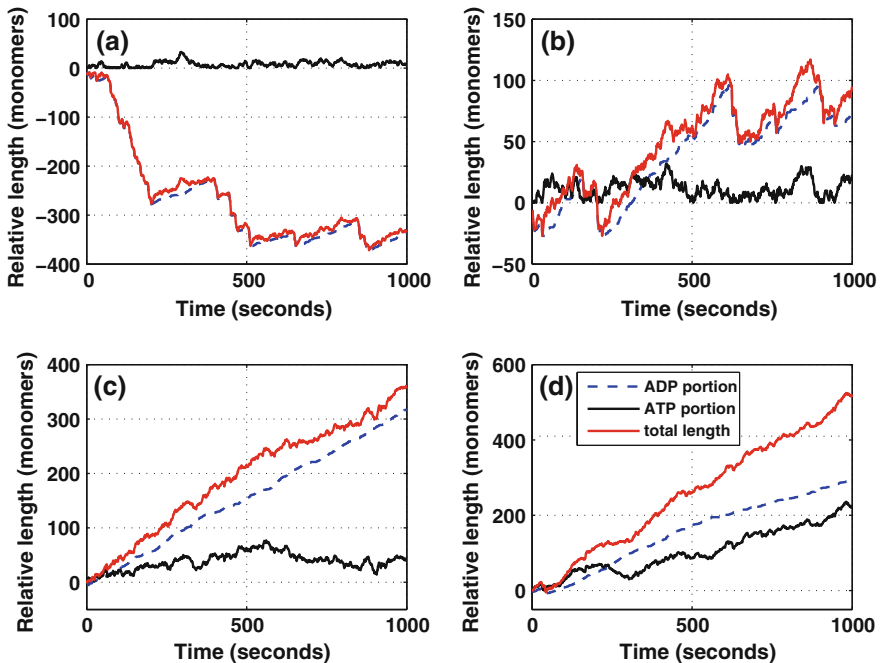


Fig. 9 One stochastic realization showing the filament fluctuations at various fixed G-ATP concentrations for a long filament initially composed of G-ADP only. The y-axis represents transient length of ADP-, ATP-portion and whole filament relative to their initial sizes. The kinetic rate constants are as in Fig. 6, except (a) $k_T^+c = 1.5 \text{ s}^{-1}$, (b) $k_T^+c = 1.68 \text{ s}^{-1}$, (c) $k_T^+c = 1.7 \text{ s}^{-1}$, (d) $k_T^+c = 1.75 \text{ s}^{-1}$

agrees with the filament length fluctuations in a closed system shown in Fig. 1. Thus the ATP cap fluctuations produce large filament length fluctuations, which indicates a mild dynamic instability in actin filament polymerization.

5 The three-state filament model

5.1 The master equation

In this section we investigate single filament polymerization in a system of fixed composition of actin monomers and incorporate all three nucleotides. We assume that both filament ends are active and we suppose that the concentrations of ADP-, ADP-Pi- and ATP-G-actin are c_1, c_2, c_3 , respectively, and are constant (the alternate case of a closed system with total monomer numbers fixed and transitions between the three nucleotide-bearing monomers incorporated was studied in Matzavinos and Othmer (2007)). We denote the on- and off-rates of the three-state actin at the barbed end as $k_b^{\pm 1}, k_b^{\pm 2}, k_b^{\pm 3}$, respectively, and the corresponding rates at the pointed end as $k_p^{\pm 1}, k_p^{\pm 2}, k_p^{\pm 3}$, respectively. Within a filament, the uniform random hydrolysis rate is denoted by r_h , and the subsequent Pi release rate is denoted by r_i .

We identify a single filament by a sequence of nucleotide types, where ADP, ADP-Pi and ATP are denoted as 1, 2, 3, respectively. A typical filament of length n can be viewed as $(a_1 a_2 \dots a_n)$, where a_i indicates the nucleotide type of the i -th subunits counted from the barbed end, i.e., a_1 denotes the nucleotide associated with the barbed end. We group all the nucleotide states into triads and order them as follows:

$$\begin{aligned}
 n = 1 & : [(1) (2) (3)] \\
 n = 2 & : [(11) (21) (31)]; [(12) (22) (32)]; [(13) (23) (33)] \\
 n = 3 & : [(111) (211) (311)]; [(121) (221) (321)]; [(131) (231) (331)]; \\
 & [(112) (212) (312)]; [(122) (222) (322)]; [(132) (232) (332)]; \\
 & [(113) (213) (313)]; [(123) (223) (323)]; [(133) (233) (333)]; \\
 & \vdots
 \end{aligned}$$

One can generate a triad of length n from one of length $n - 1$, call it $(a_1 a_2 \dots a_{N-1})$, by addition at the barbed end to give $3(N - 1)$ triads of the form

$$[(1a_1 a_2 \dots a_{N-1}), (2a_1 a_2 \dots a_{N-1}), (3a_1 a_2 \dots a_{N-1})]$$

and another group of triads can be generated by addition to the pointed end. Similarly, one can generate triads of length n from those of length $n + 1$ by truncation at either end.

We store the probabilities of the different nucleotide sequences of length n , ordered as above, in the column vector P^n . For instance,

$$\begin{aligned}
 P^1 & = (p(1), p(2), p(3))^T \\
 P^2 & = (p(11), p(21), p(31), p(12), p(22), p(32), p(13), p(23), p(33))^T
 \end{aligned}$$

where $p(a_1 a_2 \dots a_n, t)$ represents the probability of a filament with the particular nucleotide sequence $(a_1 a_2 \dots a_n)$ at time t (hereafter we suppress t).

In a system in which the monomer concentrations are constant, both filament ends can undergo stochastic elongation and shrinkage, and the time evolution of the probability P^n is given by

$$\frac{dP^n}{dt} = U_{n-1} P^{n-1} + L_{n+1} P^{n+1} - D_n P^n + H_n P^n \tag{210}$$

Here the ‘raising’ operator U_{n-1} and the ‘lowering’ operator L_{n+1} are defined as

$$\begin{aligned}
 U_{n-1} & = \mathbf{I}_{3^{n-1}} \otimes (k_b^{+1} c_1 \quad k_b^{+2} c_2 \quad k_b^{+3} c_3)^T + (k_p^{+1} c_1 \quad k_p^{+2} c_2 \quad k_p^{+3} c_3)^T \otimes \mathbf{I}_{3^{n-1}} \\
 L_{n+1} & = (\mathbf{I}_{3^n} \otimes (k_b^{-1} \quad k_b^{-2} \quad k_b^{-3}) + (k_p^{-1} \quad k_p^{-2} \quad k_p^{-3}) \otimes \mathbf{I}_{3^n})
 \end{aligned}$$

where the tensor product of matrices is multiplication of elements of the first factor by the second factor (Othmer and Scriven 1971). The diagonal operator D , which both

converts nucleotides within a triad of length n and converts triads of length n to those of length $n \pm 1$ by addition or truncation is defined as

$$D_n = \begin{pmatrix} k_b^{+1} + k_p^{+1} \\ k_b^{+1} + k_p^{+2} \\ k_b^{+1} + k_p^{+3} \end{pmatrix}^T \cdot \begin{pmatrix} c_1 \\ c_2 \\ c_3 \end{pmatrix} \mathbf{I}_{3^n} \\ + \mathbf{I}_{3^{n-1}} \otimes \begin{pmatrix} k_b^{-1} & & \\ & k_b^{-2} & \\ & & k_b^{-3} \end{pmatrix} + \begin{pmatrix} k_p^{-1} & & \\ & k_p^{-2} & \\ & & k_p^{-3} \end{pmatrix} \otimes \mathbf{I}_{3^{n-1}}$$

The hydrolysis term is a collection of hydrolysis and Pi release reactions on all subunits as

$$H_n = \sum_{i=0}^{n-1} \mathbf{I}_{3^i} \otimes (\mathbf{R} \otimes \mathbf{I}_{3^{n-1-i}})$$

where

$$R = \begin{pmatrix} 0 & r_i & 0 \\ 0 & -r_i & r_h \\ 0 & 0 & -r_h \end{pmatrix}$$

The probability vector comprised of the P^n s for $n = 1, 2, \dots$ is denoted

$$P = (P^{1T}, P^{2T}, P^{3T}, P^{4T}, \dots)^T$$

and it evolves according to

$$\frac{dP}{dt} = K P \tag{211}$$

where the infinite constant matrix K is given by

$$K = \begin{pmatrix} H_1 - D_1 & L_2 & & & & \\ U_1 & H_2 - D_2 & L_3 & & & \\ & U_2 & H_3 - D_3 & L_4 & & \\ & & U_3 & H_4 - D_4 & L_5 & \\ & & & & & \ddots \end{pmatrix}$$

We remark that in the above expression the hydrolysis and Pi release are assumed to be the same for both terminal and interior subunit. The evolution of the mean and

variance of the length distribution are governed by

$$j = \frac{dM}{dt} = \frac{d}{dt} \left(\sum_n n P_n \right) \quad (212)$$

$$D = \frac{d\sigma^2}{dt} = \frac{d}{dt} \left(\sum_n n^2 P_n - \left(\sum_n n P_n \right)^2 \right) \quad (213)$$

where P_n is the sum of all components of P^n .

5.2 Numerical simulations

Though the dynamics of the length and nucleotide composition of a single filament can be described in the compact mathematical form given at (211), it is not feasible to solve this analytically, and thus we resort to numerical solutions. We use the algorithm developed earlier for stochastic simulation of filament dynamics (Matzavinos and Othmer 2007).

Different polymerization models have been proposed in the literature, depending on the kinetics of G-ADP-Pi and Pi release at the filament ends. Some have proposed that G-ADP-Pi is kinetically identical to G-ATP, while others argue that their dynamics are significantly different. Another open question is whether the inorganic Pi of ADP-Pi is released significantly faster at the terminal subunit than at the interior subunits. Here we will examine the long-time elongation and fluctuations of filament polymerization using the most recent kinetic model proposed by Fujiwara et al. (2007). In this model, the off rates of G-ADP-Pi at both ends are surprisingly small and the phosphate is released more rapidly at the terminal ADP-Pi-actin than at the interior monomers. We also examine the effects of end capping and Pi release rate of the terminal subunit on the long-time behavior of elongation and length fluctuation by blocking the pointed ends and suppressing the terminal Pi release. The monomer pool is assumed to be composed of a constant concentration of G-ATP. The long-time elongation and length diffusion constants for each model are displayed in Fig. 10.

Interestingly, we observe that capping of the pointed end does not significantly affect the long-time behavior of filament polymerization when Pi is released rapidly at the tip, as is seen by a comparison of Model I and the 'pointed-end-blocked' Model III in Fig. 10. This is mainly due to the relatively slow dynamics of the pointed end compared to those at the barbed end. However, both the elongation and diffusion curves change significantly when Pi in a monomer at the barbed end is released at the same slow rate as from the interior subunits, as seen by comparing Model I and II. The slow Pi release decreases the critical concentration of G-ATP, and produces surprisingly high fluctuations at a G-ATP concentration slightly less than the critical concentration. With slow Pi release at the tip, the filament tip is presumably stabilized since the dynamics of ADP-Pi-actin is extremely slow. We also re-examine a kinetic model used by Vavylonis et al. (2005) wherein G-ADP-Pi behaves similar to G-ATP and Pi release is slow at the barbed end. In all these models, we observed a non-monotonic

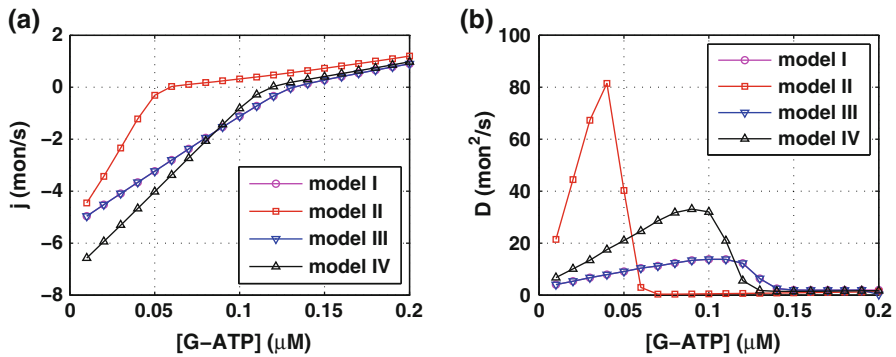


Fig. 10 The asymptotic elongation rate (a) and diffusion constant (b) of actin filaments at various fixed G-ATP concentrations. Both the elongation rate and the diffusion constant are averaged over 4,000 realizations. Model-I: full three state model with kinetic rate constant shown in Fig. 2 from Pollard (2007), with both ends free and rapid Pi release at the tip ($r_i = 2 \text{ s}^{-1}$); Model-II: same as Model I, but with uniform slow Pi release ($r_i = 0.003 \text{ s}^{-1}$); Model-III: same as Model I, but with only the barbed end free and rapid Pi release at the tip; Model-IV: three-state filament with only barbed end free, uniform slow Pi release and kinetic rate constants from Vavylonis et al. (2005). Note that results from Model I and III are indistinguishable in the figure

dependence of the filament growth rate around the critical concentration, and in particular, a tooth-shaped diffusion curve occurs at concentrations below the critical value. By comparing Figs. 8 and 10, we conclude that the two-state filament model captures the non-monotonic feature of the full three-state model, and the large length fluctuations result from the intermittent capping of filament ends by dynamically distinct G-ATP monomers.

6 Discussion

We have developed and analyzed in detail a polymerization model involving two monomer types A and B as depicted in Fig. 4, in which A serves as a cap on a B filament, since B does not add to an A end-monomer. We analytically derived the length distribution and the first two moments of this distribution for the A- and B-components of the filaments, as well as for the entire filament. We find that the evolution of filament length is distinctly different above and below the critical concentration for A, and in particular, the diffusion coefficient is discontinuous there. We also show that the elongation rate and the filament length diffusion rate converge to a steady state at a rate that can be given explicitly in terms of the on- and off-rates (see (65)). By setting the on-rate of the B-monomer to zero, we obtain the asymptotic elongation and length diffusion rate constants for an actin filament as shown in Fig. 11. On either side of the critical concentration, the curves of elongation rate and diffusion constant are linear with respect to actin monomer concentration, but both curves are of different slopes above and below the critical value. While the elongation rate is continuous at the critical concentration, the diffusion constant exhibits a large drop there.

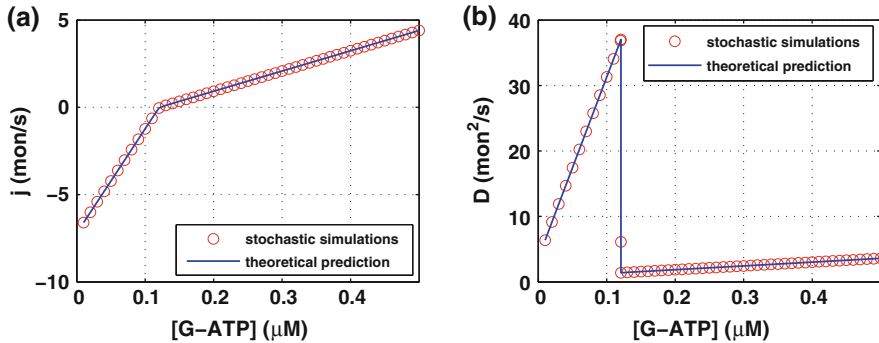


Fig. 11 The elongation rate **(a)** and diffusion constant **(b)** of the filament barbed end at large times. The kinetic constants used in the simulations are: $k_T^+ = 11.6 \mu M s^{-1}$, $k_T^- = 1.4 s^{-1}$, $k_D^- = 7.2 s^{-1}$. The circles represent results of stochastic simulations, whereas the line is predicted according to (98), (104) and (121)

When there is no cap on a pure-B filament the filament tip executes a biased random walk, and the stationary drift and diffusion rates, $r - s$ and $(r + s)/2$, respectively, can be computed from a simple biased random walk. Addition of an A-monomer interrupts this and the interplay between the two processes produces the complex dependence of the diffusion rate on the A and B on- and off-rates. We show that when $\alpha < \beta$, the steady-state cap size distribution is exponential with a finite mean length. Equations (100) and (101) suggest that the length fluctuations in this case are mainly due to the dynamic change of the B core, which is consistent with the fact that the cap size stabilizes at large times. In the presence of A, the filament switches randomly between the capped and uncapped states, and when the off-rate is higher than the on-rate (i.e. $\alpha < \beta$), the filament has a probability $1 - \alpha/\beta$ of being uncapped. It was shown that the mean elongation rate of the single filament is the elongation rate of an uncapped filament ($r - s$) times the probability that the filament is uncapped. However, the effective diffusion of the filament is much more complicated, and involves both a weighted diffusive component and a scaled convective component. As shown in Eq. (99), the diffusion coefficient is comprised of that for the uncapped filament times the probability of being uncapped, plus a term in the drift of the B-segment squared times a factor involving the probability of being capped. If the polymerization of uncapped filament is not biased (i.e. the on-rate of B equals the off-rate), the contribution of the second term in the effective diffusion vanishes, as does the drift. Then the capping simply reduces the effective diffusion. In addition, when the ratio α/β is held constant, the diffusion rate constant is a monotone decreasing function of β . When β is held constant, the diffusion constant is a quadratic function of α . As shown earlier, the asymptotic dynamics of a single filament can also be modeled as two-state random walk.

On the other hand, when $\alpha > \beta$, the probability P_m of a cap of finite size vanishes as $t \rightarrow \infty$, and the cap simply grows. The B core is capped by A most of the time, and thus the length fluctuations of the filament are mainly due to the cap. The filament length change is thus reduced to the behavior of single-state filament model. The difference in the dynamics for $\alpha > \beta$ (supercritical A) and $\alpha < \beta$ (subcritical A)

is reflected in the fact that the diffusion coefficient at the critical concentration differs from the limits from above and below, as shown in Fig. 11.

The full three monomer-type model can only be treated computationally, but the results are broadly consistent with those of the two-type model, which indicates that the latter captures the essential features of the dynamics.

The current two-state polymer model can be extended to investigate filament growth subjected to an imposed force simply by incorporating the force dependence of addition and release in the on- and off-rates. Other potential applications involve the ‘hopping’ of signaling molecules along a cell surface, in the axon of neurons, and between binding sites in fluorescence assays.

Acknowledgments This work was supported by NIH grant GM29123, NSF grants DMS-0517884 and DMS-0817529, and the University of Minnesota Supercomputing Institute.

References

- Abramowitz M, Stegun I (1965) Handbook of mathematical functions
 Alexander M, Oster G (1996) Cell motility driven by actin polymerization. *Biophys J* 71(6):3030–3045
 Bugyi B, Carlier MF (2010) Control of actin filament treadmilling in cell motility. *Annu Rev Biophys* 39:449–470
 Carlier MF, Pantaloni D, Korn ED (1986) The effects of Mg²⁺ at the high-affinity and low-affinity sites on the polymerization of actin and associated ATP hydrolysis. *J Biol Chem* 261:10785–10792
 Carlsson AE (2008) Model of reduction of actin polymerization forces by ATP hydrolysis. *Phys Biol* 5(3): 1–9
 De La Cruz EM (2009) How cofilin severs an actin filament. *Biophys Rev* 1:51–59
 Dickinson RB, Caro L, Purich DL (2004) Force generation by cytoskeletal filament end-tracking proteins. *Biophys J* 87:2838–2854
 Doorn van EA (2001) Representations for the rate of convergence of birth-death processes. Memorandum No. 1584, University of Twente
 Fass J, Pak C, Bamberg J, Mogilner A (2008) Stochastic simulation of actin dynamics reveals the role of annealing and fragmentation. *J Theor Biol* 252(1):173–183
 Footer MJ, Kerssemakers JWJ, Theriot JA, Dogterom M (2007) Direct measurement of force generation by actin filament polymerization using an optical trap. *PNAS* 104(7):2181–2186
 Fujiwara I, Takahashi S, Tadakuma H, Funatsu T, Ishiwata S (2002) Microscopic analysis of polymerization dynamics with individual actin filaments. *Nat Cell Biol* 4(9):666–673
 Fujiwara I, Vavylonis D, Pollard TD (2007) Polymerization kinetics of adp- and adp-pi-actin determined by fluorescence microscopy. *PNAS* 104(21):8827–8832
 Goel NS, Richter-Dyn N (1974) Stochastic models in biology. Academic, New York
 Hill TL (1986) Theoretical study of a model for the ATP cap at the end of an actin filament. *Biophys J* 49(5):981–986
 Hotulainen P, Hoogenraad CC (2010) Actin in dendritic spines: connecting dynamics to function. *J Cell Biol* 189(4):619–629
 Hu J, Matzavinos A, Othmer HG (2007) A theoretical approach to actin filament dynamics. *J Stat Phys* 128(1–2):111–138
 Kuhn JR, Pollard TD (2005) Real-time measurements of actin filament polymerization by total internal reflection fluorescence microscopy. *Biophys J* 88(2):1387–1402
 Marcy Y, Prost J, Carlier MF, Sykes C (2004) Forces generated during actin-based propulsion: a direct measurement by micromanipulation. *PNAS* 101(16):5992–5997
 Matzavinos A, Othmer HG (2007) A stochastic analysis of actin polymerization in the presence of twinfilin and gelsolin. *J Theor Biol* 249(4):723–736
 McGrath JL, Osborn EA, Tardy YS, Dewey CF Jr, Hartwig JH (2000) Regulation of the actin cycle in vivo by actin filament severing. *PNAS* 97(12):6532–6537
 Mitchison T, Kirschner M (1984) Dynamic instability of microtubule growth. *Nature* 312:237–242

- Oosawa F, Asakura S (1975) Thermodynamics of the Polymerization of Protein. Academic Press
- Othmer HG, Scriven LE (1971) Instability and dynamic pattern in cellular networks. *J Theor Biol* 32:507–537
- Pollard TD, Borisy GG (2003) Cellular motility driven by assembly and disassembly of actin filaments. *Cell* 112(4):453–465
- Pollard TD (2007) Regulation of actin filament assembly by arp2/3 complex and formins. *Annu Rev Biophys Biomol Struct* 36:451–477
- Ponti A, Machacek M, Gupton SL, Waterman-Storer CM, Danuser G (2004) Two distinct actin networks drive the protrusion of migrating cells. *Science* 305:1782–1786
- Popp D, Yamamoto A, Iwasa M, Narita A, Maeda K, Maéda Y (2007) Concerning the dynamic instability of actin homolog ParM. *Biochem Biophys Res Commun* 353(1):109–114
- Ranjith P, Lacoste D, Mallick K, Joanny JF (2009) Nonequilibrium self-assembly of a filament coupled to ATP/GTP hydrolysis. *Biophys J* 96(6):2146–2159
- Ranjith P, Mallick K, Joanny JF, Lacoste D (2010) Role of ATP-hydrolysis in the dynamics of a single actin filament. *Biophys J* 98(8):1418–1427
- Schaus TE, Borisy GG (2008) Performance of a population of independent filaments in lamellipodial protrusion. *Biophys J* 95(3):1393–1411
- Stukalin EB, Kolomeisky AB (2006) ATP hydrolysis stimulates large length fluctuations in single actin filaments. *Biophys J* 90(8):2673–2685
- Theriot JA, Mitchison TJ (1991) Actin microfilament dynamics in locomoting cells. *Nature* 352:126–131
- Tolic-Nørrelykke IM (2010) Force and length regulation in the microtubule cytoskeleton: lessons from fission yeast. *Curr Opin Cell Biol* 22(1):21–28
- VanBuren V, Cassimeris L, Odde DJ (2005) Mechanochemical model of microtubule structure and self-assembly kinetics. *Biophys J* 89(5):2911–2926
- Vavylonis D, Yang Q, O’Shaughnessy B (2005) Actin polymerization kinetics, cap structure, and fluctuations. *PNAS* 102(24):8543–8548
- Weiss GH (1976) The two-state random walk. *J Stat Phys* 15(2):157–165
- Zigmond SH (1993) Recent quantitative studies of actin filament turnover during locomotion. *Cell Motil Cytoskeleton* 25:309–316